eLIFE elifesciences.org

RESEARCH ARTICLE

Biophysical mechanisms in the mammalian respiratory oscillator re-examined with a new data-driven computational model

Ryan S Phillips[1,2], Tibin T John[1], Hidehiko Koizumi[1], Yaroslav I Molkov[3,4], Jeffrey C Smith[1]*

[1]Cellular and Systems Neurobiology Section, National Institute of Neurological Disorders and Stroke, National Institutes of Health, Bethesda, United States; [2]Department of Physics, University of New Hampshire, Durham, United States; [3]Department of Mathematics and Statistics, Georgia State University, Atlanta, United States; [4]Neuroscience Institute, Georgia State University, Atlanta, United States

Abstract An autorhythmic population of excitatory neurons in the brainstem pre-Bötzinger complex is a critical component of the mammalian respiratory oscillator. Two intrinsic neuronal biophysical mechanisms—a persistent sodium current (I_{NaP}) and a calcium-activated non-selective cationic current (I_{CAN})—were proposed to individually or in combination generate cellular- and circuit-level oscillations, but their roles are debated without resolution. We re-examined these roles in a model of a synaptically connected population of excitatory neurons with I_{CAN} and I_{NaP}. This model robustly reproduces experimental data showing that rhythm generation can be independent of I_{CAN} activation, which determines population activity amplitude. This occurs when I_{CAN} is primarily activated by neuronal calcium fluxes driven by synaptic mechanisms. Rhythm depends critically on I_{NaP} in a subpopulation forming the rhythmogenic kernel. The model explains how the rhythm and amplitude of respiratory oscillations involve distinct biophysical mechanisms.
DOI: https://doi.org/10.7554/eLife.41555.001

***For correspondence:** smithj2@ninds.nih.gov

Competing interests: The authors declare that no competing interests exist.

Funding: See page 23

Received: 04 September 2018
Accepted: 07 February 2019
Published: 25 March 2019

Reviewing editor: Jan-Marino Ramirez, Seattle Children's Research Institute and University of Washington, United States

Introduction

Defining cellular and circuit mechanisms generating the vital rhythm of breathing in mammals remains a fundamental unsolved problem of wide-spread interest in neurophysiology (***Richter and Smith, 2014***; ***Del Negro et al., 2018***; ***Ramirez and Baertsch, 2018a***), with potentially far-reaching implications for understanding mechanisms of oscillatory circuit activity and rhythmic motor pattern generation in neural systems (***Marder and Calabrese, 1996***; ***Buzsaki, 2006***; ***Grillner, 2006***; ***Kiehn, 2006***). The brainstem pre-Bötzinger complex (pre-BötC) region (***Smith et al., 1991***) located in the ventrolateral medulla oblongata is established to contain circuits essential for respiratory rhythm generation (***Smith et al., 2013***; ***Del Negro et al., 2018***), but the operational cellular biophysical and circuit synaptic mechanisms are continuously debated. Pre-BötC excitatory neurons and circuits have autorhythmic properties and drive motor circuits that can be isolated and remain rhythmically active in living rodent brainstem slices in vitro. Numerous experimental and theoretical analyses have focused on the rhythmogenic mechanisms operating in these in vitro conditions to provide insight into biophysical and circuit processes involved, with potential relevance for rhythm generation during breathing in vivo (***Feldman and Del Negro, 2006***; ***Lindsey et al., 2012***; ***Richter and Smith, 2014***; ***Ramirez and Baertsch, 2018b***). The ongoing rhythmic activity in vitro has been suggested to arise from a variety of cellular and circuit biophysical mechanisms including from a subset(s) of intrinsically bursting neurons which, through excitatory synaptic interactions, recruit

and synchronize neurons within the network (pacemaker-network models) (**Butera et al., 1999b**; **Ramirez et al., 2004**; **Toporikova and Butera, 2011**; **Chevalier et al., 2016**), or as an emergent network property through recurrent excitation (e.g. **Rekling and Feldman, 1998**; **Jasinski et al., 2013**) and/or synaptic depression (group pacemaker model) (**Rubin et al., 2009a**; **Del Negro et al., 2010**).

From these previous analyses, involvement of two possible cellular-level biophysical mechanisms have been proposed. One based on a slowly inactivating persistent sodium current (I_{NaP}) (**Butera et al., 1999a**), and the other on a calcium-activated non-selective cation current (I_{CAN}) coupled to intracellular calcium ($[Ca]_i$) dynamics (for reviews see **Rybak et al., 2014**; **Del Negro et al., 2010**), or a combination of both mechanisms (**Thoby-Brisson and Ramirez, 2001**; **Jasinski et al., 2013**; **Peña et al., 2004**). Despite the extensive experimental and theoretical investigations of these sodium- and calcium-based mechanisms, the actual roles of I_{NaP}, I_{CAN} and the critical source(s) of $[Ca]_i$ transients in the pre-BötC are still unresolved. Furthermore, in pre-BötC circuits, the process of rhythm generation must be associated with an amplitude of circuit activity sufficient to drive downstream circuits to produce adequate inspiratory motor output. Biophysical mechanisms involved in generating the amplitude of pre-BötC circuit activity have also not been established.

I_{NaP} is proposed to mediate an essential oscillatory burst-generating mechanism since pharmacologically inhibiting I_{NaP} abolishes intrinsic neuronal rhythmic bursting as well as pre-BötC circuit inspiratory activity and rhythmic inspiratory motor output in vitro (**Koizumi et al., 2008**; **Toporikova et al., 2015**), although some studies suggest that block of both I_{NaP} and I_{CAN} are necessary to disrupt rhythmogenesis in vitro (**Peña et al., 2004**). Theoretical models of cellular and circuit activity based on I_{NaP}-dependent bursting mechanisms closely reproduce experimental observations such as voltage-dependent frequency control, spike-frequency adaptation during bursts, and pattern formation of inspiratory motor output (**Butera et al., 1999b**; **Pierrefiche et al., 2004**; **Smith et al., 2007**). This indicates the plausibility of I_{NaP}-dependent rhythm generation.

In the pre-BötC, I_{CAN} was originally postulated to underlie intrinsic pacemaker-like oscillatory bursting at the cellular level and contribute to circuit-level rhythm generation, since intrinsic bursting in a subset of neurons in vitro was found to be terminated by the I_{CAN} inhibitor flufenamic acid (FFA) (**Peña et al., 2004**). Furthermore, inhibition of I_{CAN} in the pre-BötC reduces the amplitude of the rhythmic depolarization (inspiratory drive potential) driving neuronal bursting and can eliminate inspiratory motor activity in vitro (**Pace et al., 2007**). I_{CAN} became the centerpiece of the 'group pacemaker' model for rhythm generation, in which this conductance was proposed to be activated by inositol trisphosphate (IP3) receptor/ER-mediated intracellular calcium fluxes initiated via glutamatergic metabotropic receptor-mediated signaling in the pre-BötC excitatory circuits (**Del Negro et al., 2010**). The molecular correlate of I_{CAN} was postulated to be the transient receptor potential channel M4 (TRPM4) (**Mironov, 2008**; **Pace et al., 2007**), one of the two known Ca^{2+}-activated TRP channels (**Guinamard et al., 2010**; **Ullrich et al., 2005**), or alternatively, by the transient receptor potential channels C3/7 (TRPC3/7) (**Ben-Mabrouk and Tryba, 2010**); however, these latter channels are not known to be Ca^{2+}-activated (**Clapham, 2003**). TRPM4 and TRPC3 have now been identified by immunolabeling and RNA expression profiling in pre-BötC inspiratory neurons in vitro (**Koizumi et al., 2018**).

Investigations into the sources of intracellular Ca^{2+} activating I_{CAN}/TRPM4 suggested that (1) somatic calcium transients from voltage-gated sources do not contribute to the inspiratory drive potential (**Morgado-Valle et al., 2008**), (2) IP3/ER-mediated intracellular Ca^{2+} release does not contribute to inspiratory rhythm generation in vitro, and (3) in the dendrites calcium transients may be triggered by excitatory synaptic inputs and travel in a wave propagated to the soma (**Mironov, 2008**). Theoretical studies have demonstrated the plausibility of $[Ca]_i$-I_{CAN}-dependent bursting (**Rubin et al., 2009b**; **Toporikova and Butera, 2011**); however, these models omit I_{NaP} and/or depend on additional unproven mechanisms to generate intracellular calcium oscillations to provide burst termination, such as IP3-dependent calcium-induced calcium release (**Toporikova and Butera, 2011**), partial depolarization block of action potentials (**Rubin et al., 2009a**), and the Na^+/K^+ pump (**Jasinski et al., 2013**). Interestingly, pharmacological inhibition of I_{CAN}/TRPM4 has been shown to produce large reductions in the amplitude of pre-BötC inspiratory neuron population activity with essentially no, or minor perturbations of inspiratory rhythm (**Peña et al., 2004**). These observations constrain the role of I_{CAN}, and require theoretical re-examination of pre-BötC neuronal conductance

mechanisms and network dynamics, particularly how rhythm generation mechanisms can be independent of I_{CAN}-dependent mechanisms that regulate the amplitude of network activity.

In this theoretical study, we examine the role of I_{CAN} in pre-BötC excitatory circuits by considering two plausible mechanisms of intracellular calcium fluxes: (1) from voltage-gated and (2) from synaptically activated sources. We deduce that I_{CAN} is primarily activated by calcium transients that are coupled to rhythmic excitatory synaptic inputs originating from I_{NaP}-dependent bursting inspiratory neurons. Additionally, we show that I_{CAN} contributes to the inspiratory drive potential by mirroring the excitatory synaptic current. This concept is consistent with a mechanism underlying generation of the inspiratory drive potential involving a synaptic-based I_{CAN} activation described in previous work (***Pace et al., 2007***; ***Rubin et al., 2009a***). Our model explains the experimental observations obtained from in vitro neonatal rodent slices isolating the pre-BötC, showing large reductions in network activity amplitude by inhibiting I_{CAN}/TRPM4 without perturbations of inspiratory rhythm generation in pre-BötC excitatory circuits in vitro. The model supports the concept that I_{CAN} activation in a subpopulation of pre-BötC excitatory neurons is critically involved in amplifying synaptic drive from a subset of neurons whose rhythmic bursting is critically dependent on I_{NaP} and forms the kernel for rhythm generation in vitro. The model suggests how the functions of generating the rhythm and amplitude of inspiratory oscillations in pre-BötC excitatory circuits are determined by distinct biophysical mechanisms.

Results

$\bar{g}_{CAN}$ variation has opposite effects on amplitude and frequency of network bursting in the Ca_V and Ca_{Syn} models

Experimental work (***Peña et al., 2004***) has demonstrated that pharmacological inhibition of I_{CAN}/TRPM4 in the pre-BötC from in vitro neonatal mouse/rat slice preparations, strongly reduces the amplitude of (or completely eliminates) the inspiratory hypoglossal (XII) motor output, as well as the amplitude of pre-BötC excitatory circuit activity that is highly correlated with the decline of XII activity, while having relatively little effect on inspiratory burst frequency. Here, we systematically examine in our model the relationship between I_{CAN} conductance ($\bar{g}_{CAN}$) and the amplitude and frequency of network activity for voltage-gated (Ca_V) and synaptically activated sources (Ca_{Syn}) of intracellular calcium in a heterogeneous network of 100 synaptically coupled single-compartment pre-BötC model excitatory neurons. In addition to voltage-gated and synaptically activated calcium currents, each model neuron incorporates voltage-gated action potential generating currents, as well as I_{CAN}, I_{NaP}, leak, and excitatory synaptic currents adapted from the conductance-based biophysical model of ***Jasinski et al. (2013)*** (see Materials and methods for a full model description). We note that in our full model, I_{CAN} is activated by both voltage-gated and synaptic mechanisms, consistent with experimental results (***Thoby-Brisson and Ramirez, 2001***; ***Pace et al., 2007***; ***Morgado-Valle et al., 2008***). Initial separate consideration of the Ca_V and Ca_{Syn} provides a means to deduce the relative contribution of these two general sources of intracellular calcium to I_{CAN} activation. We found that reduction of $\bar{g}_{CAN}$ drives opposing effects on network activity amplitude (spike/s/neuron) and frequency that are dependent on the source of intracellular calcium transients (***Figure 1***). The network activity amplitude is a measure of the average neuronal population firing rate and is defined by the number of spikes generated by the network per 50 ms bin divided by the number of neurons in the network. In the Ca_V network, where calcium influx is generated exclusively from voltage-gated calcium channels, increasing $\bar{g}_{CAN}$ has no effect on amplitude but increases the frequency of network oscillations (***Figure 1A, C, D***). Conversely, in the Ca_{Syn} network where calcium influx is generated exclusively by excitatory synaptic input, increasing $\bar{g}_{CAN}$ strongly increases the amplitude and slightly decreases the oscillation frequency (***Figure 1B, C, D***).

Effects of subthreshold activation of I_{CAN} on network frequency

In I_{NaP}-dependent bursting neurons in the pre-BötC, bursting frequency depends on their excitability (i.e. baseline membrane potential) which can be controlled in different ways, for example by directly injecting a depolarizing current (***Smith et al., 1991***; ***Del Negro et al., 2005***; ***Yamanishi et al., 2018***) or varying the conductance and/or reversal potentials of some ionic channels (***Butera et al., 1999a***).

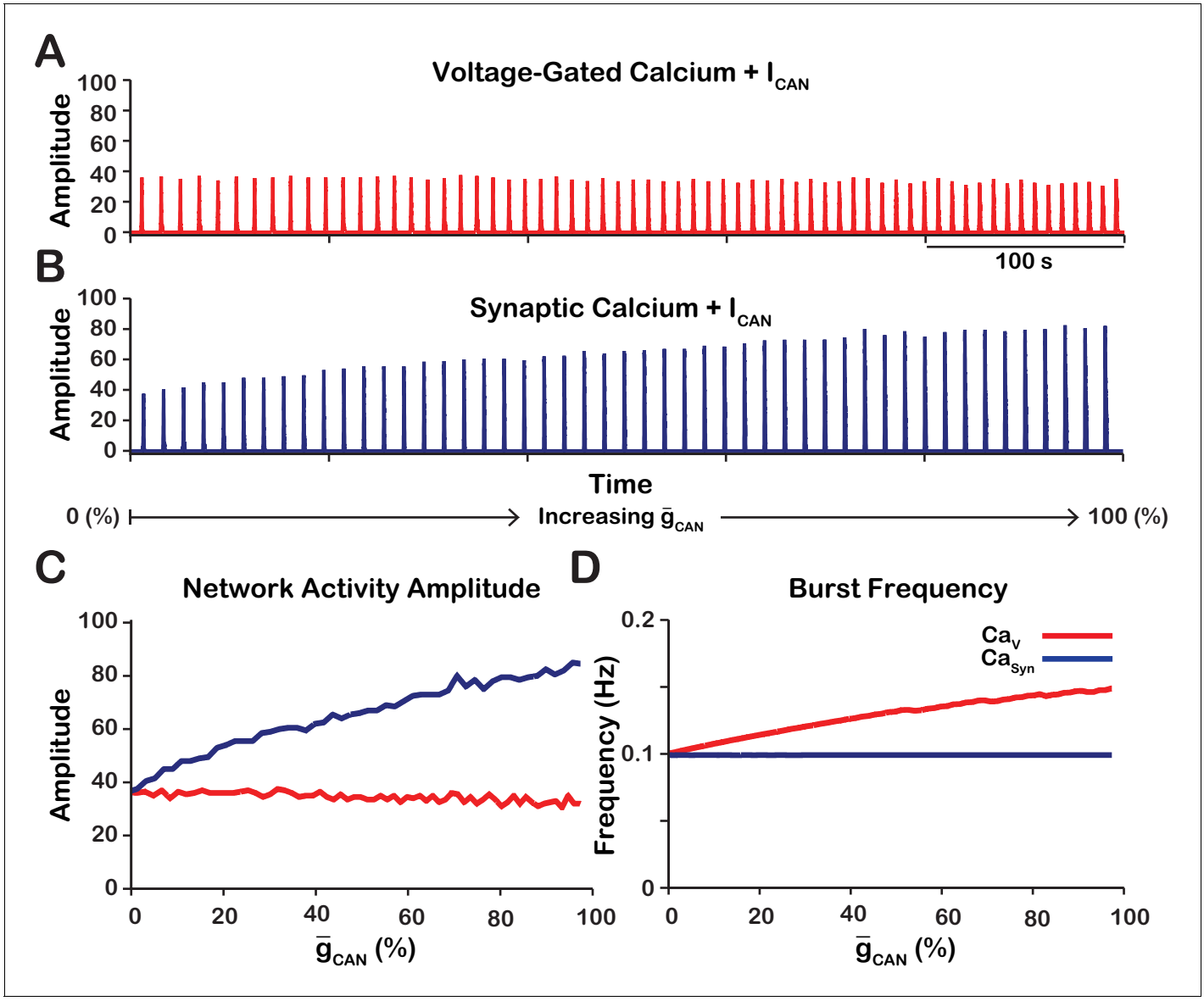

Figure 1. Manipulations of $\bar{g}_{CAN}$ in the Ca_V and Ca_{Syn} networks produce opposite effects on network activity amplitude (spikes/s) and frequency. (**A** and **B**) Histograms of neuronal population activity amplitude in the Ca_V, and Ca_{Syn} networks with linearly increasing $\bar{g}_{CAN}$. (**C**) Plot of $\bar{g}_{CAN}$ (% of the baseline mean value for the simulated population) vs. network activity amplitude for the Ca_V and Ca_{Syn} networks in A and B. (**D**) Plot of $\bar{g}_{CAN}$ (%) vs. network frequency for the Ca_V and Ca_{Syn} networks in A and B. Ca_V network parameters: $\bar{g}_{Ca} = 1.0$ (nS), $P_{Ca} = 0.0$, $P_{Syn} = 0.05$ and $W_{max} = 0.2$ (nS). Ca_{Syn} network parameters: $\bar{g}_{Ca} = 0$ (nS), $P_{Ca} = 0.01$, $P_{Syn} = 0.05$ and $W_{max} = 0.2$ (nS).

DOI: https://doi.org/10.7554/eLife.41555.002

Due to their relatively short duty cycle, the bursting frequency in these neurons is largely determined by the interburst interval, defined as the time between the end of one burst and the start of the next. During the burst, I_{NaP} slowly inactivates (***Butera et al., 1999a***) resulting in burst termination and abrupt neuronal hyperpolarization. The interburst interval is then determined by the amount of time required for I_{NaP} to recover from inactivation and return the membrane potential back to the threshold for burst initiation. This process is governed by the kinetics of I_{NaP} inactivation gating variable h_{NaP}. Higher neuronal excitability reduces the value of h_{NaP} required to initiate bursting. Consequently, the time required to reach this value is decreased, which results in a shorter interburst interval and increased frequency.

To understand how changing $\bar{g}_{CAN}$ affects network bursting frequency, we quantified the values of h_{NaP} averaged over all rhythm-generating pacemaker neurons immediately preceding each network burst and, also, the average I_{CAN} values between the bursts in the Ca_V and Ca_{syn} networks (***Figure 2***). In the Ca_V network, I_{Ca} as modeled remains residually activated between the bursts thus creating the background calcium concentration which partially activates I_{CAN}. Therefore, between the bursts I_{CAN} functions as a depolarizing leak current. Consistently, we found that in the Ca_V network increasing $\bar{g}_{CAN}$ increases I_{CAN} (***Figure 2A***), progressively depolarizing the network, which reduces the h_{NaP} threshold for burst initiation (***Figure 2B***) and, thus, increases network oscillation frequency (***Figure 1D***).

In the Ca_{syn} model, the intracellular calcium depletes entirely during the interburst interval. Consequently, increasing $\bar{g}_{CAN}$ has no effect on I_{CAN} (***Figure 2A***) and frequency is essentially unaffected (***Figure 1D***).

Changes in network activity amplitude are driven by recruitment of neurons

As previously stated, the network activity amplitude is defined as the total number of spikes produced by the network per a time bin divided by the number of neurons in the network. Consequently, changes in amplitude can only occur by increasing the number of neurons participating in bursts (recruitment) and/or increasing the firing rate of the recruited neurons. To analyze changes in amplitude, we quantified the number of recruited neurons (***Figure 3A***) and the average spike frequency in recruited neurons (***Figure 3B***) as a function of $\bar{g}_{CAN}$ for both network models. In the Ca_V network, increasing $\bar{g}_{CAN}$ increases the number of recruited neurons (***Figure 3A***), but decreases the average spiking frequency in recruited neurons (***Figure 3B***) which, together result in no change in amplitude (***Figure 1C***). In the Ca_{Syn} network, increasing $\bar{g}_{CAN}$ strongly increases the number of recruited neurons (***Figure 3A***) and increases the spike frequency of recruited neurons (***Figure 3B***) resulting in a large increase in network activity amplitude (***Figure 3C***).

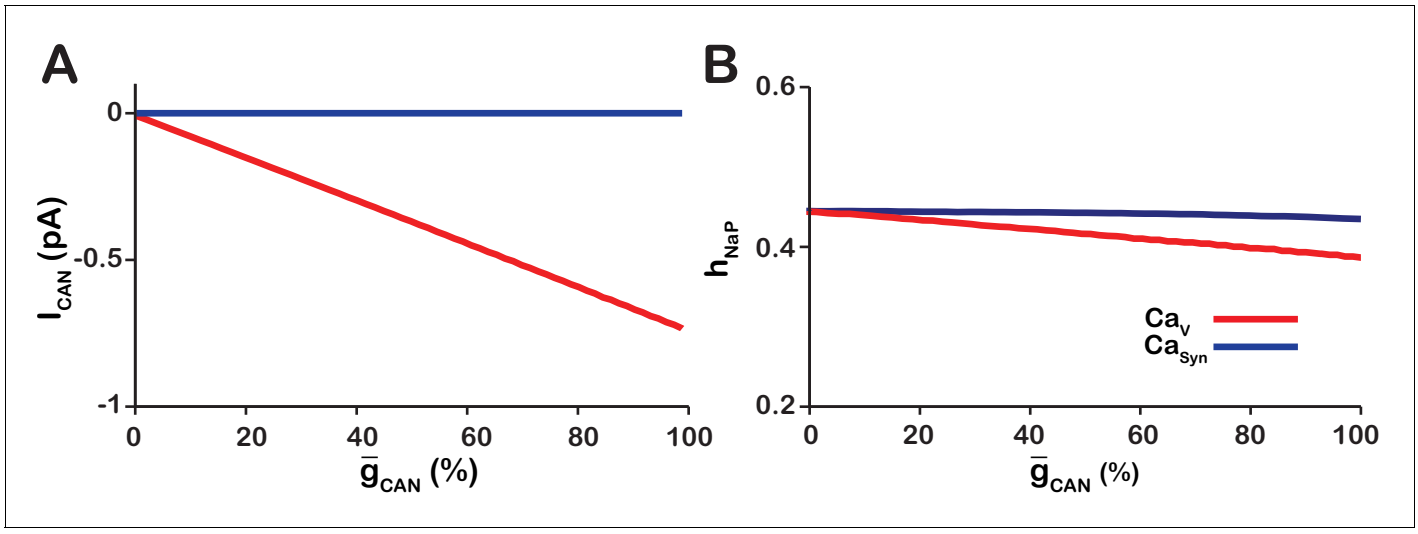

Figure 2. Calcium source and $\bar{g}_{CAN}$-dependent effects on cellular properties regulating network frequency for the simulations presented in ***Figure 1***. (**A**) Average magnitude of I_{CAN} in pacemaker neurons during the interburst interval for the Ca_V (red) and Ca_{Syn} (blue) networks. (**B**) Average inactivation (h_{NaP}) of the burst generating current I_{NaP} in pacemaker neurons immediately preceding each network burst as a function of $\bar{g}_{CAN}$ (%) for the voltage-gated and synaptic calcium networks. Ca_V network parameters: $\bar{g}_{Ca} = 1.0$ (nS), $P_{Ca} = 0.0$, $P_{Syn} = 0.05$ and $W_{max} = 0.2$ (nS). Ca_{Syn} network parameters: $\bar{g}_{Ca} = 0$ (nS), $P_{Ca} = 0.01$, $P_{Syn} = 0.05$ and $W_{max} = 0.2$ (nS).

DOI: https://doi.org/10.7554/eLife.41555.003

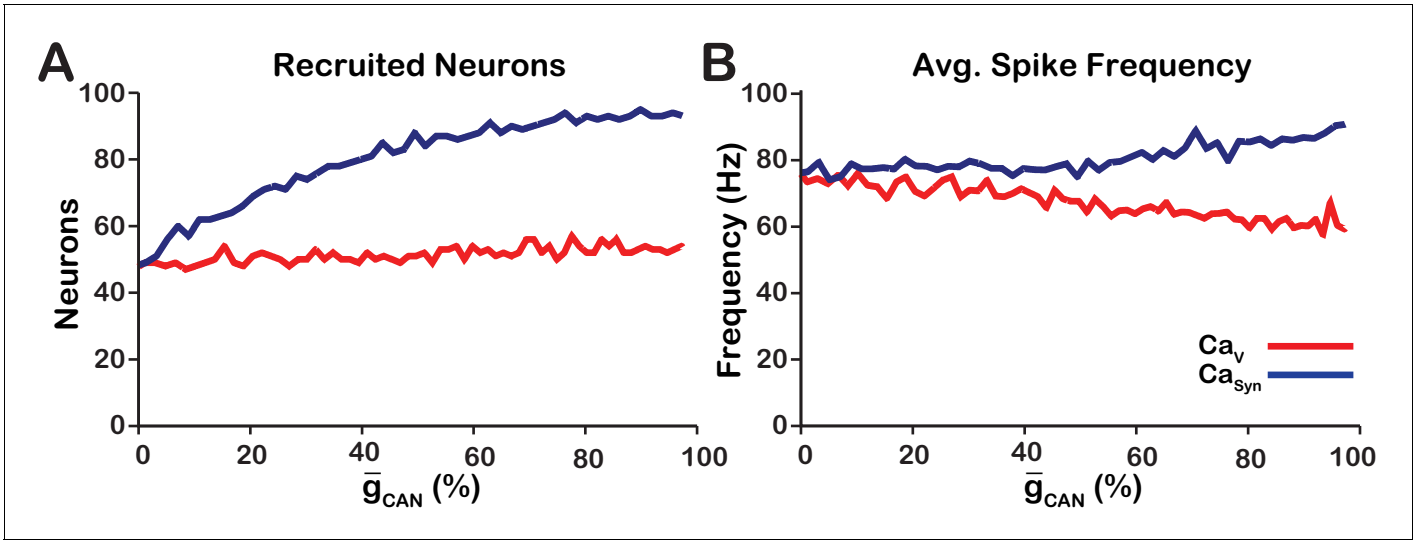

Figure 3. Calcium source and $\bar{g}_{CAN}$-dependent effects on cellular properties regulating network activity amplitude for the simulations presented in *Figure 1*. (**A**) Number of recruited neurons in the modeled population of 100 neurons as a function of $\bar{g}_{CAN}$ (%) for voltage-gated and synaptic calcium sources. The number of recruited neurons is defined as the peak number of spiking neurons per bin during a network burst. (**B**) Average spiking frequency of recruited neurons as a function of $\bar{g}_{CAN}$ for the voltage-gated and synaptic calcium mechanism. Average spiking frequency is defined the number of spikes per bin divided by the number of recruited neurons. The parameters used in these simulations are: $\boldsymbol{Ca_V}$: $\bar{g}_{Ca} = 1.0$ $(\boldsymbol{nS})$, $\boldsymbol{P_{Ca}} = 0.0$, $\boldsymbol{P_{Syn}} = 0.05$ and $\boldsymbol{W_{max}} = 0.2$ $(\boldsymbol{nS})$. $\boldsymbol{Ca_{Syn}}$: $\bar{g}_{Ca} = 0$ $(\boldsymbol{nS})$, $\boldsymbol{P_{Ca}} = 0.01$, $\boldsymbol{P_{Syn}} = 0.05$ and $\boldsymbol{W_{max}} = 0.2$ $(\boldsymbol{nS})$.

DOI: https://doi.org/10.7554/eLife.41555.004

Manipulating $\bar{g}_{CAN}$ in the Ca_{Syn} model is qualitatively equivalent to changing the strength of synaptic interactions

Since changes in $\bar{g}_{CAN}$ in the Ca_{Syn} model primarily affect network activity amplitude through recruitment of neurons, and the network activity amplitude strongly depends on the strength of synaptic interactions, we next examined the relationship between $\bar{g}_{CAN}$, synaptic strength and network activity amplitude and frequency (*Figure 4*). Synaptic strength is defined as the number of neurons multiplied by the synaptic connection probability multiplied by the average weight of synaptic connections ($N \cdot P_{Syn} \cdot \frac{1}{2} W_{max}$), where the weight of synaptic connections W_{max} ranges from 0.0 to 1.0 nS. We found that the effects of varying $\bar{g}_{CAN}$ or the synaptic strength on network activity amplitude and frequency are qualitatively equivalent in the Ca_{Syn} network which is indicated by symmetry of the heat plots (across the X=Y line) in *Figure 4A,B*. This symmetry results from the fact that the effective strength of synaptic interactions in the network is roughly proportional to a product of the synaptic strength and $\bar{g}_{CAN}$. A transition from bursting to tonic spiking occurs when this effective excitation exceeds a certain critical value. This is why the bifurcation curve corresponding to a transition from rhythmic bursting to tonic spiking (a boundary between yellow and black in *Figure 4A*) looks like a hyperbola ($\bar{g}_{CAN} \times synaptic\ strength = const$).

We further investigated and compared the effect of reducing $\bar{g}_{CAN}$ or the synaptic strength on network activity amplitude and frequency as well as the effects on the recruitment of neurons not involved in rhythm generation (*Figure 4C–F*). To make this comparison, we picked a starting point in the 2D parameter space of $\bar{g}_{CAN}$ and synaptic strength where the network is bursting. Then in separate simulations, we gradually reduced either $\bar{g}_{CAN}$ or the synaptic strength to zero. We show that reducing either $\bar{g}_{CAN}$ or the synaptic strength have very similar effects on network activity amplitude and frequency (*Figure 4C,D*). Furthermore, de-recruitment of neurons in both cases is nearly identical (*Figure 4E,F*). Reducing either $\bar{g}_{CAN}$ or the synaptic strength decreases the excitatory input to the neurons during network oscillations which is a major component of the inspiratory drive potential. Therefore, in the Ca_{Syn} network, manipulations of $\bar{g}_{CAN}$ will affect the strength of the inspiratory drive potential in the rhythmic inspiratory neurons in a way that is equivalent to changing the synaptic

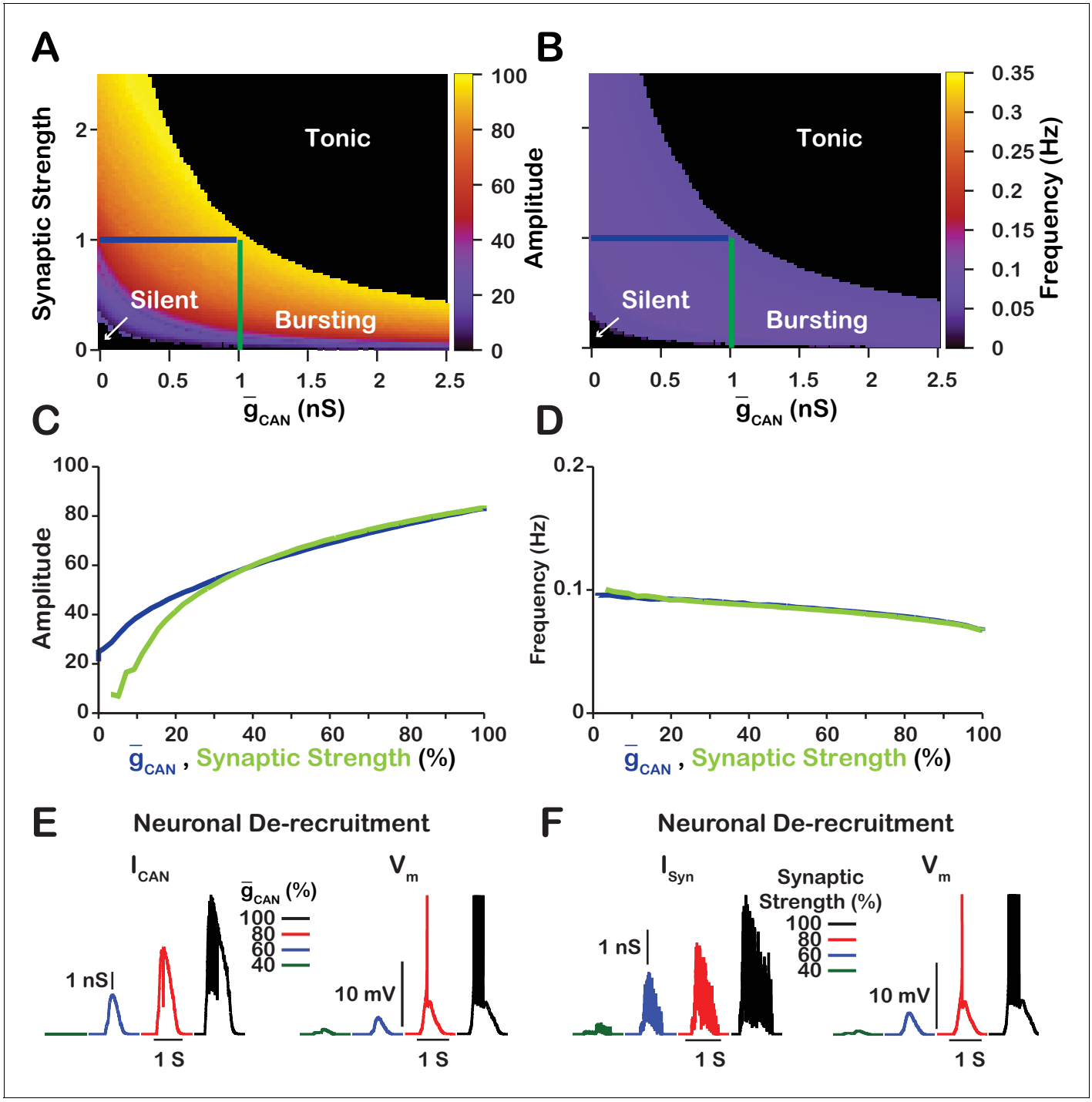

Figure 4. Manipulations of synaptic strength ($N \cdot P_{Syn} \cdot \frac{1}{2} W_{max}$) and $\bar{g}_{CAN}$ have equivalent effects on network activity amplitude, frequency and recruitment of inspiratory neurons not involved in rhythm generation. (**A** and **B**) Relationship between $\bar{g}_{CAN}$ (mean values for the simulated populations), synaptic strength and the amplitude and frequency in the Ca_{Syn} network. Notice the symmetry about the X=Y line in panels A and B, which, indicates that changes in $\bar{g}_{CAN}$ and or synaptic strength are qualitatively equivalent. Synaptic strength was changed by varying W_{max}. (**C**) Relationship between network activity amplitude and the reduction of $\bar{g}_{CAN}$ (blue) or synaptic strength (green). (**D**) Relationship between network frequency and the reduction of $\bar{g}_{CAN}$ (blue) or synaptic strength (green). (**E** and **F**) Decreasing $\bar{g}_{CAN}$ or synaptic strength de-recruits neurons by reducing the inspiratory drive potential, indicated by the amplitude of subthreshold depolarization, right traces. The solid blue and green lines in panels A and B represent the location in the 2D parameter space of the corresponding blue and green curves in C and D. The action potentials in the right traces of E and F are

Figure 4 continued on next page

Figure 4 continued

truncated to show the change in neuronal inspiratory drive potential. The parameters used for these simulations are $\boldsymbol{Ca_{Syn}}$: $\bar{\boldsymbol{g}}_{\boldsymbol{Ca}} = [0, 0]$, $\boldsymbol{P_{Ca}} = 0.01$, $\boldsymbol{P_{Syn}} = 1.0$ and $\boldsymbol{W_{max}} = \boldsymbol{var}$.

DOI: https://doi.org/10.7554/eLife.41555.005

strength of the network. In contrast, manipulations of $\bar{g}_{CAN}$ in the Ca_V network will only slightly affect the inspiratory drive potential due to changes in the average firing rate of active neurons (see ***Figure 3B***).

Robustness of amplitude and frequency effects

We also examined if the effects are conserved in both the Ca_V and Ca_{Syn} networks over a range of network parameters. To test this, we investigated the dependence of network activity amplitude and frequency on $\bar{g}_{CAN}$ and average synaptic strength for Ca_{Syn} and Ca_V networks with high ($P_{Syn} = 1$) and low ($P_{Syn} = 0.05$) connection probabilities, and high ($g_{Ca} = 0.1\ nS,\ P_{Ca} = 0.1$), medium ($g_{Ca} = 0.01\ nS,\ P_{Ca} = 0.01$) and low ($g_{Ca} = 0.001\ nS,\ P_{Ca} = 0.005$) strengths of calcium sources (***Figure 5*** and ***6***). We found that changing the synaptic connection probability and changing the strength

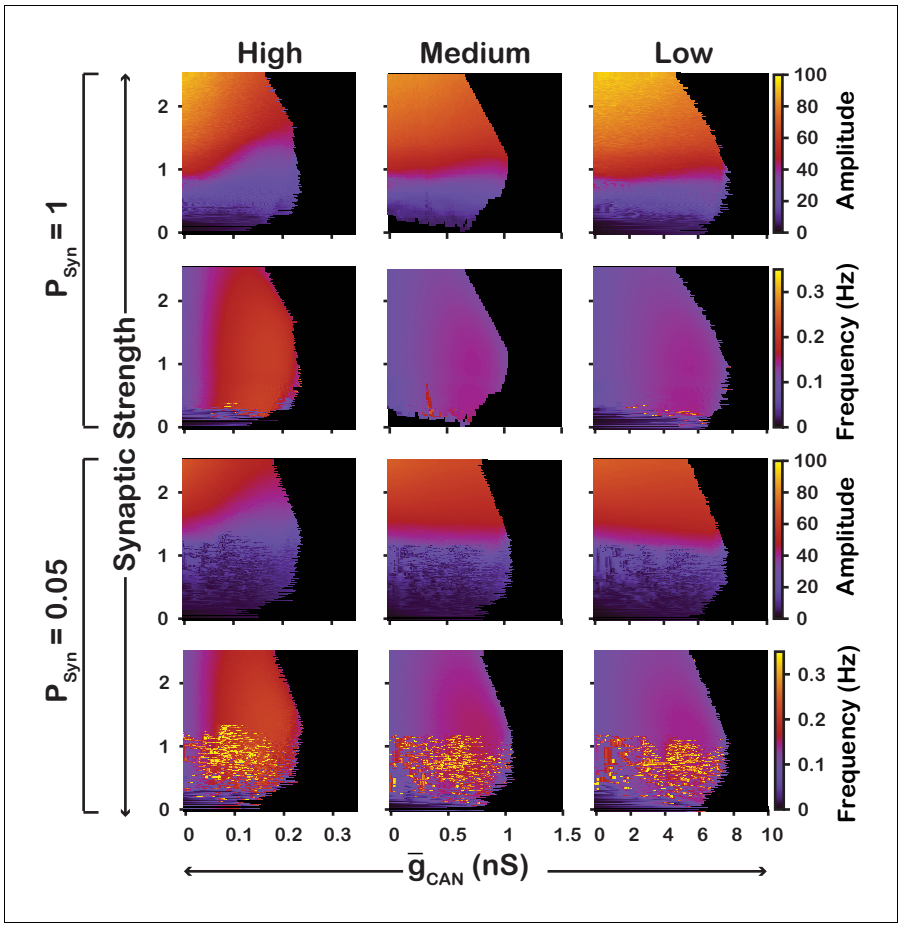

Figure 5. Robustness of amplitude and frequency effects to changes in $\bar{\boldsymbol{g}}_{\boldsymbol{CAN}}$ and synaptic strength in the $\boldsymbol{Ca_V}$ network for 'high' (left), 'medium' (middle) and 'low' (right) conductance of the voltage-gated calcium channel $\boldsymbol{I_{Ca}}$ as well as 'high' (top) and 'low' (bottom) network connection probabilities. Amplitude and frequency are indicated by color (scale bar at right). Black regions indicate tonic network activity. Values of $\bar{\boldsymbol{g}}_{\boldsymbol{CAN}}$ indicated are the mean values for the simulated neuronal populations.

DOI: https://doi.org/10.7554/eLife.41555.006

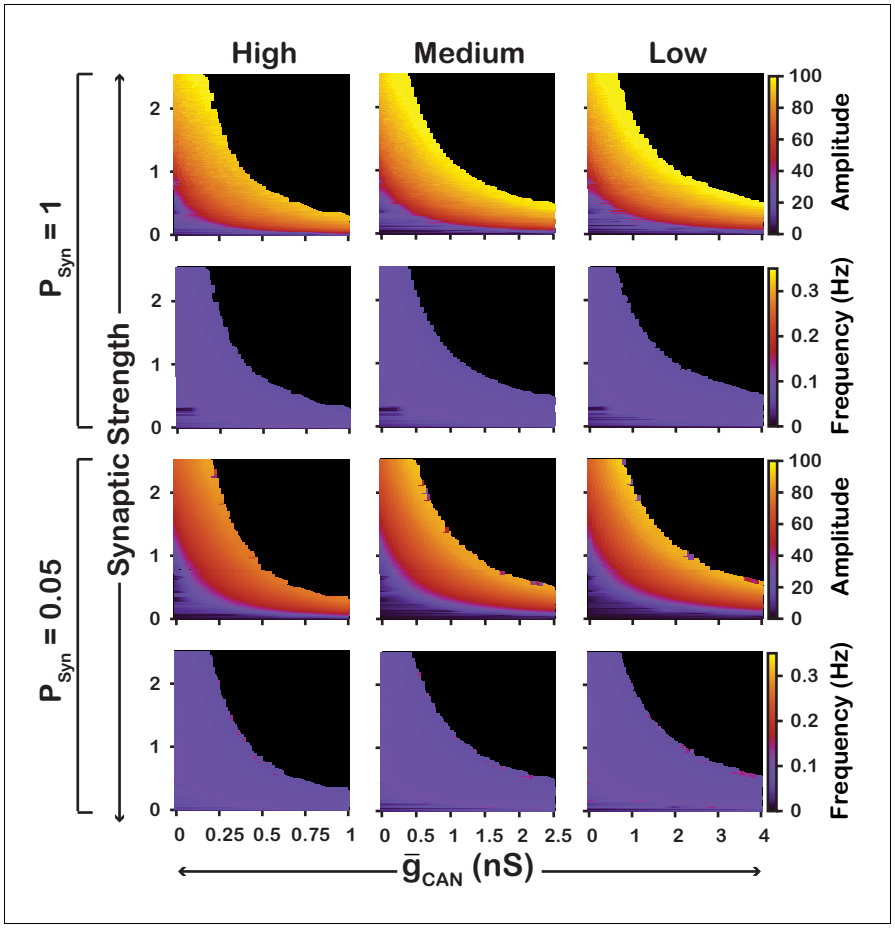

Figure 6. Robustness of amplitude and frequency effects to changes in $\bar{g}_{CAN}$ and synaptic strength in the Ca_{Syn} network for 'high' (left), 'medium' (middle) and 'low' (right) calcium conductance in synaptic currents as well as 'high' (top) and 'low' (bottom) network connection probabilities. Amplitude and frequency are indicated by color (scale bar at right). Black regions indicate tonic network activity. Values of $\bar{g}_{CAN}$ indicated are the mean values for the simulated neuronal populations.

DOI: https://doi.org/10.7554/eLife.41555.007

of the calcium sources has no effect on the general relationship between $\bar{g}_{CAN}$ and the amplitude or frequency of bursts in the Ca_V or Ca_{Syn} networks. In other words, the general effect of increasing $\bar{g}_{CAN}$ on amplitude and frequency is conserved in both networks regardless of the synaptic connection probability or strength of the calcium sources. Increasing the strength of the calcium sources does, however, affects the range of possible $\bar{g}_{CAN}$ values where both networks produce rhythmic activity.

To summarize, in the Ca_V model, increasing $\bar{g}_{CAN}$ increases frequency, through increased excitability but has no effect on amplitude. In contrast, in the Ca_{Syn} model, increasing $\bar{g}_{CAN}$ slightly decreases frequency and increases amplitude. In this case, increasing $\bar{g}_{CAN}$ acts as a mechanism to increase the inspiratory drive potential and recruit previously silent neurons. Additionally, these features of the Ca_V and Ca_{Syn} models are robust and conserved across a wide range of network parameters.

Intracellular calcium transients activating I_{CAN} primarily result from synaptically activated sources

In experiments where I_{CAN}/TRPM4 was blocked by bath application of FFA or 9-phenanthrol (***Koizumi et al., 2018***) in vitro, the amplitude of network oscillations was strongly reduced and their frequency remained unchanged or was reduced insignificantly. Our model revealed that the effects

of I_{CAN} blockade on amplitude and frequency depend on the source(s) of intracellular calcium (see ***Figures 1*** and ***2***). If the calcium influx is exclusively voltage-gated, our model predicts that I_{CAN} blockade will have no effect on amplitude but reduce the frequency. In contrast, if the calcium source is exclusively synaptically gated, our model predicts that blocking I_{CAN} will strongly reduce the amplitude and slightly increase the frequency. Therefore, a multi-fold decrease in amplitude, seen experimentally, is consistent with the synaptically driven calcium influx mechanisms, while nearly constant bursting frequency may be due to calcium influx through both voltage- and synaptically gated channels. Following the predictions above, to reproduce experimental data, we incorporated both mechanisms in the full model and inferred their individual contributions by finding the best fit. We found that the best match is observed (***Figure 7***) if synaptically mediated and voltage-gated calcium influxes comprise about 95% and 5% of the total calcium influx, respectively. We note that some experiments have shown a small (~20%) reduction of inspiratory burst frequency accompanying larger reductions in pre-BötC population activity amplitude with I_{CAN} block (***Peña et al., 2004***). In our model, such perturbations of frequency can occur if the contribution of voltage-gated calcium influxes is larger than indicated above, or if neuronal background calcium concentration which partially activates I_{CAN} is higher than specified in the model.

I_{NaP}-dependent and $[Ca]_i$-I_{CAN}-sensitive intrinsic bursting

In our model, we included I_{NaP}, I_{CAN} as well as voltage-gated and synaptic mechanisms of Ca^{2+} influx. Activation of I_{CAN} by Ca_{Syn} is the equivalent mechanism used in computational group-pacemaker

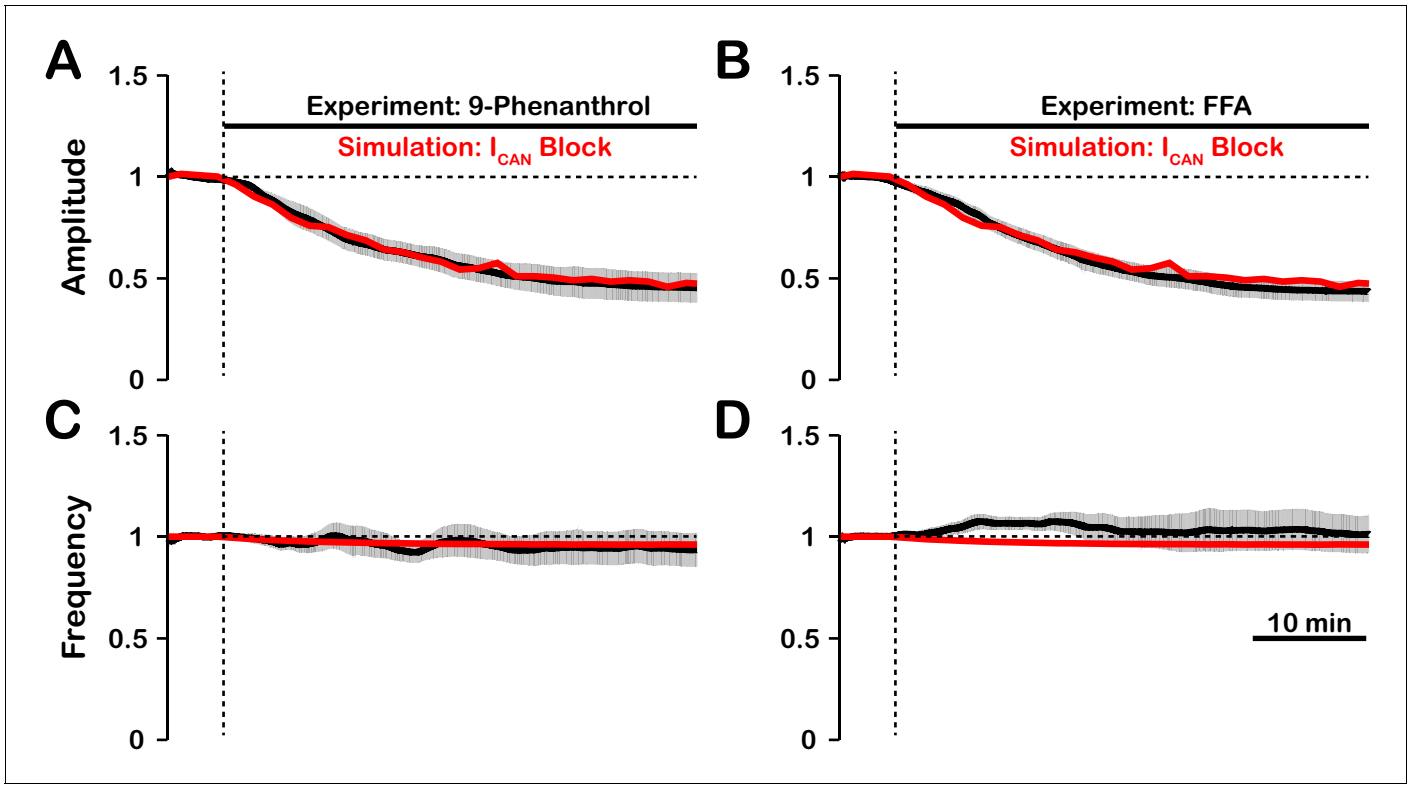

Figure 7. Experimental and simulated pharmacological blockade of I_{CAN} by (**A and C**) 9-phenanthrol and (**B and D**) flufenamic acid (FFA). Both voltage-gated and synaptic sources of intracellular calcium are included. Experimental blockade of I_{CAN} (black) by 9-phenanthrol and FFA significantly reduce the (**A and B**) amplitude of network oscillations while having little effect on (**C and D**) frequency. The black line represents the mean and the gray band is the S.E.M. of experimental integrated XII output recorded from neonatal rat brainstem slices in vitro, reproduced from ***Koizumi et al., 2018***. Simulated blockade of I_{CAN} (red) closely matches the reduction in (**A and B**) amplitude of network oscillations and slight decrease in (**C and D**) frequency seen with 9-phenanthrol and FFA. Simulated and experimental blockade begins at the vertical dashed line. Blockade was simulated by exponential decay of $\bar{g}_{CAN}$ with the following parameters: 9-phenanthrol: $\gamma_{Block} = 0.85$, $\tau_{Block} = 357s$; FFA: $\gamma_{Block} = 0.92$, $\tau_{Block} = 415s$. The network parameters are: $\bar{g}_{Ca} = 0.00175$ (nS), $P_{Ca} = 0.0275$, $P_{Syn} = 0.05$ and $W_{max} = 0.096$ (nS).

DOI: https://doi.org/10.7554/eLife.41555.008

models (*Rubin et al., 2009a*; *Song et al., 2015*). Rhythmic burst generation and termination in our model, however, are dependent on I_{NaP} (*Butera et al., 1999a*). We investigated the sensitivity of intrinsic bursting in our model to I_{NaP} and calcium channel blockade (*Figure 8*). Intrinsic bursting was identified in neurons by zeroing the synaptic weights to simulate synaptic blockade. I_{NaP} and I_{Ca} blockade was simulated by setting $\bar{g}_{NaP}$ and $\bar{g}_{Ca}$ to $0\,nS$. We found that after decoupling the network ($W_{max} = 0$) a subset of neurons remained rhythmically active (7% in this simulation) and that these were all neurons with a high I_{NaP} conductance. In these rhythmically active neurons, bursting was abolished in all neurons by I_{NaP} blockade. Interestingly, I_{Ca} blockade applied before I_{NaP} block

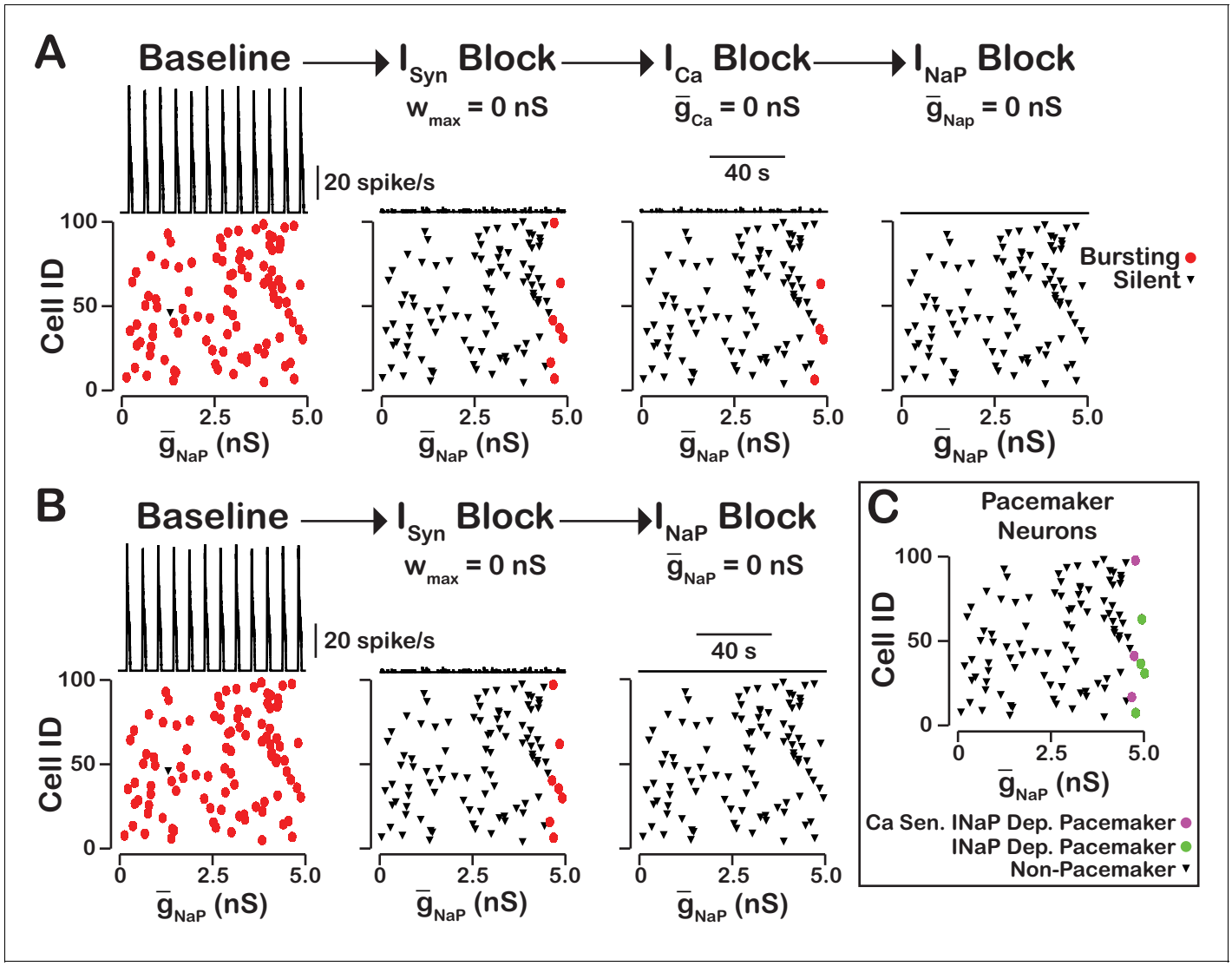

Figure 8. I_{NaP}-dependent and Ca^{2+}-sensitive intrinsic bursting. (**A**) From left to right, intrinsic bursters (pacemakers) are first identified by blocking synaptic connections. Cells whose activity is elminated under these conditions are non-pacemaker neurons. Then, calcium sensitive neurons are silenced and identified by I_{Ca} blockade. The remaining neurons are identifed as sensitive to I_{NaP} block. Top traces show the network output and Cell ID vs. $\bar{g}_{NaP}$ scatter plots that identify silent and bursting neurons under each condition. (**B**) I_{NaP} blockade after synaptic blockade eleminates bursting in all neurons. Therefore, all intrinsic bursters are I_{NaP} dependent. (**C**) Identification of calcium-sensitive and I_{NaP}-dependent as well as calcium-insensitive and I_{NaP}-dependent intrinsic bursters. Notice that only the neurons with the highest value of $\bar{g}_{NaP}$ are intrinsic bursters and that a subset of these neurons are sensitive to calcium blockade but all are dependent on I_{NaP}. The network parameters are: $\bar{g}_{Ca} = 0.00175$ (nS), $P_{Ca} = 0.0275$, $P_{Syn} = 0.05$ and $W_{max} = 0.096$ (nS). The values of $\bar{g}_{NaP}$ given in the scatter plots indicate the magnitude of $\bar{g}_{NaP}$ for each neuron in the network and show the range of the $\bar{g}_{NaP}$ distribution.

DOI: https://doi.org/10.7554/eLife.41555.009

abolished intrinsic bursting in three of the seven neurons and I_{NaP} block applied afterwards abolished intrinsic bursting in the remaining four neurons. Although only one rhythmogenic (I_{NaP}-based) mechanism exists in this model, bursting in a subset of these intrinsically bursting neurons is calcium sensitive, consistent with experimental observations of calcium-sensitive intrinsic bursters (***Thoby-Brisson and Ramirez, 2001***; ***Del Negro et al., 2005***; ***Peña et al., 2004***). In calcium-sensitive bursters, Ca^{2+} blockade in our model abolishes bursting by reducing the intracellular calcium concentration and, hence, I_{CAN} activation, which ultimately reduces excitability. We note that in our model the numbers of I_{NaP}-dependent and calcium-sensitive intrinsic bursters will vary depending on the mean and width of the I_{NaP} distribution and the background intracellular calcium concentration.

The rhythmogenic kernel

Our simulations have shown that the primary role of I_{CAN} is amplitude but not oscillation frequency modulation with little or no effect on network activity frequency. Here we examined the neurons that remain active and maintain rhythm after I_{CAN} blockade (***Figure 9***). We found that the neurons that remain active are primarily neurons with the highest $\bar{g}_{NaP}$ and that bursting in these neurons is dependent on I_{NaP}. Some variability exists and neurons with relatively low $\bar{g}_{NaP}$ value can remain active due to synaptic interactions while a neuron with a slightly higher $\bar{g}_{NaP}$ without sufficient synaptic input may become silent. These neurons that remain active after compete blockade of I_{CAN} form a I_{NaP}-dependent kernel of a rhythm generating circuit.

Intracellular calcium transients and network activity during inhibition of I_{CAN}/TRPM4

Dynamic calcium imaging has been used to assess activity of the population of pre-BöC excitatory neurons as well as individual pre-BötC neurons during pharmacological inhibition of I_{CAN}/TRPM4 in vitro (***Koizumi et al., 2018***). These experiments indicate that network output activity amplitude and pre-BötC excitatory population-level intracellular calcium transients are highly correlated while the network oscillation frequency is not significantly perturbed. Interestingly, during I_{CAN}/TRPM4 block, changes in calcium transients of individual neurons can differ significantly from the average population-level calcium transients. To assess if our model is consistent with these experimental results and

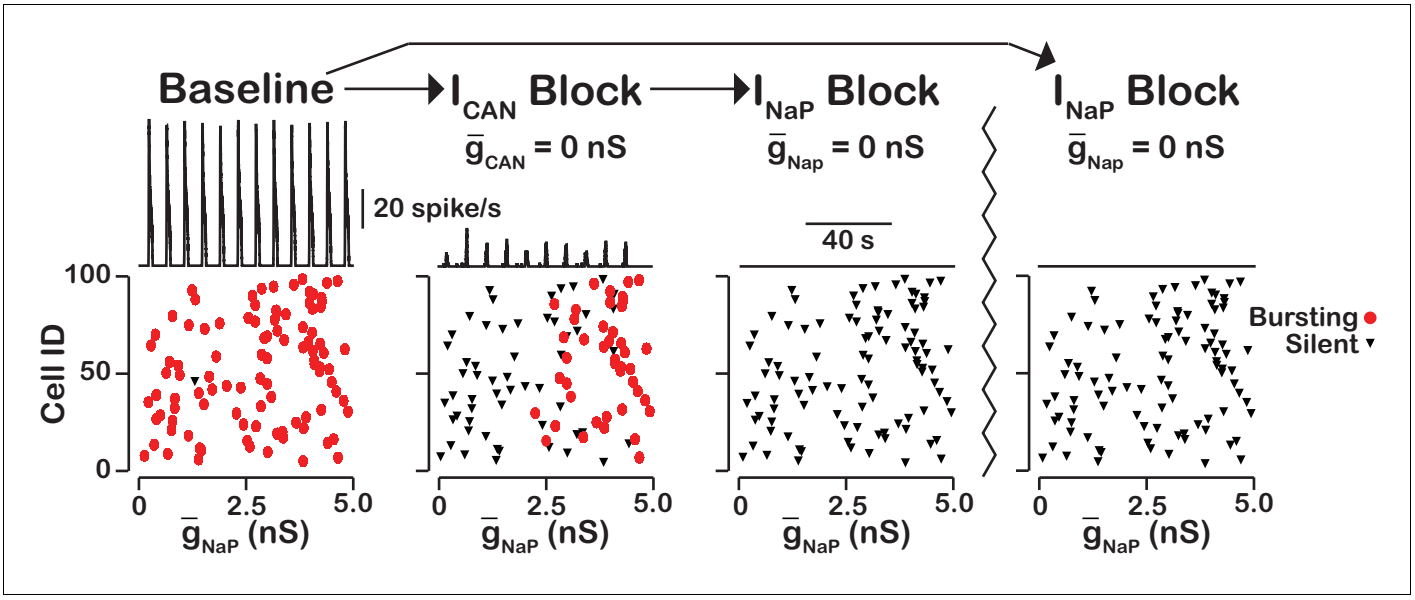

Figure 9. I_{CAN} blockade reveals an I_{NaP}-dependent rhythmogenic kernel. The top traces show the network output at baseline, after I_{CAN} blockade and I_{NaP} blockade. The bottom Cell ID vs. $\bar{g}_{NaP}$ scatter plots identify silent and bursting neurons in each conditon. Notice that only neurons with relitively high $\bar{g}_{NaP}$ remain active after I_{CAN} block. The network parameters used are: $\bar{g}_{Ca} = 0.00175$ (nS), $P_{Ca} = 0.0275$, $P_{Syn} = 0.05$ and $W_{max} = 0.096$ (nS). The values of $\bar{g}_{NaP}$ given in the scatter plots indicate the magnitude of $\bar{g}_{NaP}$ for each neuron in the network and show the range of the $\bar{g}_{NaP}$ distribution.
DOI: https://doi.org/10.7554/eLife.41555.010

gain additional insight into intracellular calcium dynamics during network activity, we analyzed simultaneous changes in the amplitude of network neuronal spiking activity, the average intracellular calcium concentration ($[Ca]_i$) of all network neurons, as well as $[Ca]_i$ of individual neurons, with different network connection probabilities (P_{Syn}) during simulated I_{CAN} block (**Figure 10**). We found that regardless of P_{Syn}, the network activity amplitude and average intracellular calcium concentration are highly correlated (**Figure 10A,B**). P_{Syn} has no effect on the relationship between amplitude, calcium transients at the network level, or network oscillation frequency provided that the synaptic strength remains constant ($N \cdot P_{Syn} \cdot \frac{1}{2} W_{max} = const$). P_{Syn} does, however, affect the change in the peak $[Ca]_i$ in individual neurons. In a network with a high connection probability ($P_{Syn} = 1$) the synaptic current/calcium transient is nearly identical for all neurons and therefore the change in $[Ca]_i$ during I_{CAN} blockade is approximately the same for each neuron (**Figure 10C**). In a sparsely connected network, as proposed for the connectivity of the pre-BötC network (**Carroll et al., 2013**; **Carroll and Ramirez, 2013**) the synaptic current and calcium influx are more variable and reflect the heterogeneity in spiking frequency of the pre-synaptic neurons (**Figure 10**). Interestingly, in a network with low connection probability ($P_{Syn}<0.1$), the peak $[Ca]_i$ transient in some neurons increases when I_{CAN} is blocked (**Figure 10E**), consistent with our experimental results (**Koizumi et al., 2018**).

Discussion

Establishing cellular and circuit mechanisms generating the rhythm and amplitude of respiratory oscillations in the mammalian brainstem pre-BötC has remained an unsolved problem of widespread interest in neurophysiology since this structure, essential for breathing to support mammalian life, was discovered nearly three decades ago (**Smith et al., 1991**). Our objective in this theoretical study was to re-examine and further define contributions of two of the main currently proposed neuronal biophysical mechanisms operating in pre-BötC excitatory circuits, specifically mechanisms involving I_{CAN} activated by neuronal calcium fluxes (**Thoby-Brisson and Ramirez, 2001**; **Peña et al., 2004**; **Del Negro et al., 2005**; **Mironov, 2008**; **Rubin et al., 2009a**) and voltage-dependent I_{NaP} in the circuit neurons (**Butera et al., 1999a**; **Del Negro et al., 2002**; **Koizumi and Smith, 2008**; **Koizumi and Smith, 2008**). While these sodium- and calcium-based mechanisms have been studied extensively over the past two-decades and shown experimentally to be integrated in pre-BötC circuits, their actual roles in circuit operation are continuously debated and unresolved (**Rybak et al., 2014**). Both mechanisms have been proposed to be fundamentally involved in rhythm generation either separately or in combination, as plausibly shown from previous theoretical modeling studies (**Butera et al., 1999a**; **Jasinski et al., 2013**; **Rubin et al., 2009a**; **Toporikova and Butera, 2011**). Furthermore, the process of rhythm generation in pre-BötC circuits must be associated with an amplitude of excitatory circuit activity sufficient to drive downstream circuits to produce adequate respiratory motor output. Biophysical mechanisms involved in generating excitatory population activity amplitude have also not been established. Our analysis is motivated by the experimental observations obtained from neonatal rodent slices isolating pre-BötC circuits in vitro that inhibition of the endogenously active I_{CAN}/TRPM4 strongly reduces the amplitude of network oscillations within pre-BötC circuits but has a small effect on oscillation frequency (**Peña et al., 2004**; **Koizumi et al., 2018**). These findings challenge currently proposed I_{CAN}-based models for rhythm generation in the isolated pre-BötC and indicate a functional organization of pre-BötC circuits, in terms of oscillatory frequency and amplitude generation, that needs to be defined.

We accordingly analyzed the role of I_{CAN} and possible sources of intracellular calcium transients activating this conductance and found that the effect of simulated I_{CAN} blockade on amplitude and frequency is highly dependent on the source(s) of intracellular calcium, which is also a central issue to be resolved. In the case where Ca_{Syn} is the primary intracellular calcium source, I_{CAN} blockade generates a large reduction in network activity amplitude. In contrast, when Ca_V is the only intracellular calcium source, I_{CAN} blockade has little effect on network activity amplitude and primarily affects the population bursting frequency that is caused by decreased excitability. Additionally, we show that activation of I_{CAN} by Ca_{Syn} functions as a mechanism to augment the inspiratory drive potential and amplitude of population activity, and that this effect is similar to increasing the synaptic coupling strength within the network. Therefore, in the case of Ca_{Syn}, blockade of I_{CAN} reduces the inspiratory drive potential causing de-recruitment of non-pacemaker rhythmic neurons and reduction of network

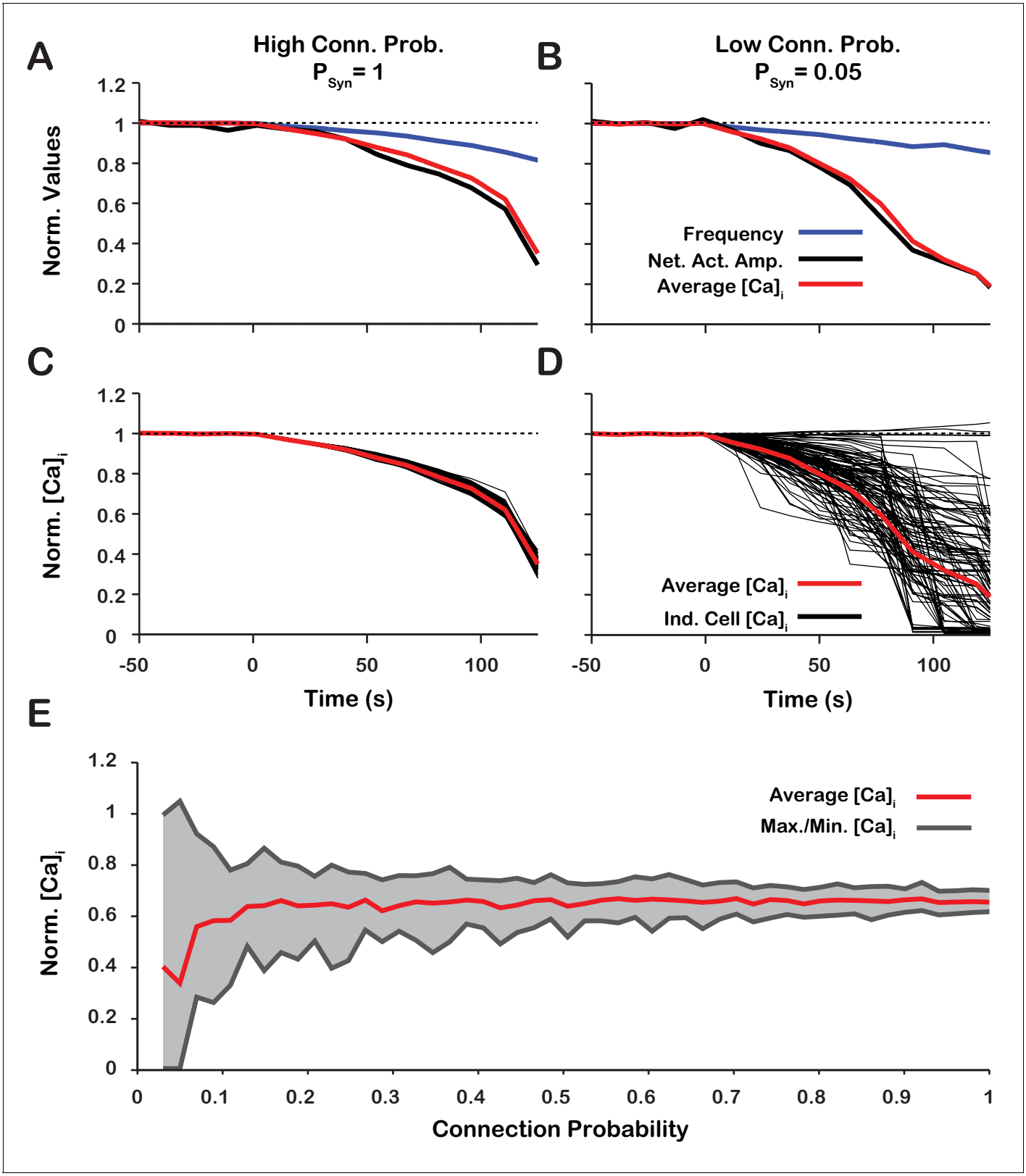

Figure 10. Changes of network activity amplitude, average network intracellular calcium concentration $[Ca]_i$ amplitude, and single model neuron $[Ca]_i$ amplitude during simulated I_{CAN} blockade. (**A and B**) Effect of I_{CAN} block on network activity amplitude, network calcium amplitude and frequency for network connection probabilities (**A**) P = 1 and (**B**) P = 0.05. (**C and D**) Effect of I_{CAN} block on changes in the magnitude of peak cellular calcium transients for network connection probabilities (**C**) $P_{Syn} = 1$ and (**D**) $P_{Syn} = 0.05$. (**E**) Maximum, minimum and average change in the peak intracellular

Figure 10 continued on next page

Figure 10 continued

calcium transient of individual neurons as a function of synaptic connection probability. All curves in A through E are normalized to their baseline values. Synaptic weight was adjusted to keep the average synaptic strength ($\boldsymbol{N \cdot P_{Syn} \cdot \frac{1}{2} W_{max} = const}$) constant. Notice that lowering the synaptic connection probability increases the variability in the peak intracellular calcium concentration during $\boldsymbol{I_{CAN}}$ blockade. Interestingly, for connection probabilities below approximately 5%, blocking $\boldsymbol{\bar{g}_{CAN}}$ can increase the peak calcium transient in a small subset of neurons. The network parameters used are: $\boldsymbol{\bar{g}_{Ca} = 0.00175\ (nS)}$ and $\boldsymbol{P_{Ca} = 0.0275}$ and $\boldsymbol{W_{max} = var}$.

DOI: https://doi.org/10.7554/eLife.41555.011

activity amplitude. In a model where I_{CAN} is activated by both Ca_V and Ca_{Syn} with contributions of 5% and 95% respectively, we show that simulated blockade of I_{CAN} generates a large reduction in network population activity amplitude and a slight decrease in frequency. This closely reproduces experimental blockade of I_{CAN}/TRPM4 by either 9-phenanthrol or FFA (***Figure 7***). Finally, we showed that the change in the peak calcium transients for individual neurons during I_{CAN} blockade, particularly at relatively low network connection probabilities ($P_{Syn} \sim <0.1$), are consistent with experimental data.

Role of I_{CAN} in the pre-BötC respiratory network

The hypothesis that I_{CAN} is involved in generation of the inspiratory rhythm is based on experimental observations from in vitro mouse medullary slice preparations (***Pace et al., 2007***; ***Mironov, 2008***; ***Del Negro et al., 2005***; ***Del Negro et al., 2010***; ***Peña et al., 2004***; ***Thoby-Brisson and Ramirez, 2001***), and in silico modeling studies (***Jasinski et al., 2013***; ***Rybak et al., 2003***; ***Toporikova and Butera, 2011***). Theories of I_{CAN}-dependent bursting rely on intracellular Ca^{2+} signaling mechanisms that have not been well defined.

Two models of I_{CAN}-dependent rhythmic bursting in vitro have been proposed and are referred to as the 'dual pacemaker' and 'group pacemaker' models. In the dual pacemaker model, two types of pacemaker neurons are proposed that are either I_{NaP}-dependent (riluzole sensitive) or I_{CAN}-dependent (Cd^{2+}sensitive) intrinsic bursters (inspiratory 'pacemaker' neurons) (see ***Rybak et al., 2014*** for review). In this model network, oscillations are thought to originate from these pacemaker neurons which through excitatory synaptic interactions synchronize bursting and drive activity of other rhythmic inspiratory neurons within the pre-BötC. Although pacemaker neurons sensitive to neuronal Ca^{2+} flux blockade through Ca_V have been reported (***Peña et al., 2004***; ***Thoby-Brisson and Ramirez, 2001***, the source and mechanism driving intracellular Ca^{2+}oscillations has not been definitely delineated. Computational models of I_{CAN}-dependent pacemaker neurons rely on mechanisms for burst initiation and termination, for example IP3-dependent Ca^{2+}oscillations (***Toporikova and Butera, 2011***; ***Del Negro et al., 2010***), that have been questioned from recent negative experimental results (***Beltran-Parrazal et al., 2012***; ***Toporikova et al., 2015***). In favor of the dual pacemaker concept, experimental evidence has been presented that pharmacological block of both I_{CAN} and I_{NaP} are necessary to disrupt rhythmogenesis under normoxic conditions in vitro (***Peña et al., 2004***). Other experimental results suggest that blocking I_{NaP} alone in vitro is sufficient (***Koizumi and Smith, 2008***; ***Toporikova et al., 2015***), and we have discussed from a theoretical perspective how such discrepancies may depend on network excitability state and connectivity (***Jasinski et al., 2013***). Our present model defines more clearly parameters such as calcium flux sources and background calcium levels that can influence the relative contributions of I_{CAN} in various network states to be further explored in model simulation studies.

In versions of the 'group pacemaker' model (***Rubin et al., 2009a***; ***Del Negro et al., 2010***; ***Feldman and Del Negro, 2006***), network oscillations are initiated through recurrent synaptic excitation that trigger postsynaptic Ca^{2+} influx. Subsequent I_{CAN} activation generates membrane depolarization (inspiratory drive potential) to drive neuronal bursting. Synaptically triggered Ca^{2+} influx and the contribution of I_{CAN} to the inspiratory drive potential of individual pre-BötC neurons are experimentally supported (***Mironov, 2008***; ***Pace et al., 2007***); however, the mechanism of burst termination remains unclear. Again, the computational group-pacemaker models that have been explored (***Rubin et al., 2009a***) rely on speculative mechanisms for burst termination that need to be tested experimentally, and in some cases lack key biophysical features of the pre-BötC neurons such as voltage-dependent frequency control and expression of I_{NaP}.

In our model, we showed that blockade of either I_{CAN} or synaptic interactions produce qualitatively equivalent effects on network population activity amplitude and frequency when the calcium transients are primarily generated from synaptic sources (***Figure 4***). Consequently, our model predicts that blockade of I_{CAN} or synaptic interactions in the isolated pre-BötC in vitro will produce comparable effects on amplitude and frequency. This is the case as ***Johnson et al. (1994)*** showed that gradual blockade of synaptic interactions by low calcium solution significantly decreases network activity amplitude while having little effect on frequency, similar to the experiments where the I_{CAN} channel TRPM4 is blocked with 9-phenanthrol (***Koizumi et al., 2018***). We note that complete blockade of I_{CAN} in our model can ultimately abolish synchronized network oscillations due to weakened excitatory synaptic transmission, which results in neuronal de-recruitment and desynchronization of the network, particularly when synaptic strength is low (***Figure 4***). Thus, I_{CAN} plays a critical role in network activity synchronization that determines the ability of the pre-BötC excitatory network to produce rhythmic output, depending on synaptic strength.

Overall, our new model simulations for the isolated pre-BötC excitatory network suggest that the role of I_{CAN}/TRPM4 activation is to amplify excitatory synaptic drive in generating the amplitude of inspiratory population activity, essentially independent of the biophysical mechanism generating inspiratory rhythm. We note that the recent experiments have also shown that in the more intact brainstem respiratory network that ordinarily generates patterns of inspiratory and expiratory activity, endogenous activation of I_{CAN}/TRPM4 appears to augment the amplitude of both inspiratory and expiratory population activity, and hence these channels are fundamentally involved in inspiratory-expiratory pattern formation (Koizumi et al., 2018).

Intracellular calcium dynamics and network activity during inhibition of I_{CAN}/TRPM4

We analyzed the correlation between calcium transients and inspiratory activity of individual inspiratory neurons as well as the entire network, particularly since dynamic calcium imaging has been utilized to assess activity of individual cells and populations of pre-BötC excitatory neurons in vitro during pharmacological inhibition of I_{CAN}/TRPM4 (***Koizumi et al., 2018***). We show that intracellular calcium transients are highly correlated with network and cellular activity across the duration of an I_{CAN} blockade simulation, consistent with experimental observations.

Additionally, we examined the relative change in the peak calcium transients in single neurons as a function of I_{CAN} conductance. We show that in a subset of neurons the peak calcium transient increases with reduced I_{CAN}. This result is surprising but is also supported by the calcium imaging data (***Koizumi et al., 2018***). This occurs in neurons that receive most of their synaptic input from pacemaker neurons and our analyses suggest this is possible in sparse networks, that is with low connection probability. In pacemaker neurons, I_{CAN} blockade leads to a reduction of their excitability resulting in an increased value of I_{NaP} inactivation gating variable at the burst onset. Thus, during the burst, the peak action potential frequency and the synaptic output from these neurons is increased with I_{CAN} blockade. Consequently, neurons that receive synaptic input from pacemaker neurons will see an increase in their peak calcium transients. In most neurons, however, synaptic input is received primarily from non-pacemaker rhythmic neurons. Since I_{CAN} blockade de-recruits these non-pacemaker neurons, the synaptic input and subsequent calcium influx in most of these cells decreases. Therefore, our model predicts that in a sparse network, which has been proposed for pre-BötC network connectivity (***Carroll et al., 2013***; ***Carroll and Ramirez, 2013***), blocking I_{CAN} results in very diverse responses at the cellular level with an overall tendency to reduce intracellular calcium transients such that the amplitude of these transients averaged over the entire population decreases during I_{CAN} blockade, while their burst frequency is essentially unchanged, as found from the calcium imaging experiments (***Koizumi et al., 2018***).

Synaptic calcium sources

Our model suggests that calcium transients in the pre-BötC are coupled to excitatory synaptic input, that is pre-synaptic glutamate release and binding to post-synaptic glutamate receptors triggers calcium entry. The specific mechanisms behind this process are unclear; however, this is likely dependent on specific types of ionotropic or metabotropic glutamate receptors.

There are three subtypes of ionotropic glutamate receptors, N-methyl-D-aspartate (NMDA), Kainate (KAR), and a-amino-3-hydroxy-5-methyl-4-isoxazolepropionic acid (AMPA), all of which are expressed in the pre-BötC (**Paarmann et al., 2000**) and have varying degrees of calcium permeability. NMDA and AMPA are unlikely candidates for direct involvement in synaptically mediated calcium influx in the pre-BötC. Pharmacological blockade of NMDA receptors does not consistently effect the amplitude or frequency of XII motor output (**Lieske and Ramirez, 2006a**; **Morgado-Valle and Feldman, 2007**; **Pace et al., 2007**) and AMPA receptors in the pre-BötC show high expression of the subunit GluR2, which renders the AMPA ion channel pore impermeable to Ca^{2+} (**Paarmann et al., 2000**). It is possible, however, that AMPA mediated depolarization may trigger calcium influx indirectly through the voltage-gated calcium channel activation on the post-synaptic terminal. The latter may contribute to synaptically triggered calcium influx as blockade of P/Q-type (but not L- N-type) calcium channels reduces XII motor output driven from the pre-BötC in the in vitro mouse slice preparations from normal animals (**Lieske and Ramirez, 2006a**; **Koch et al., 2013**).

Calcium permeability through KAR receptors is dependent on subunit expression. The KAR subunit GluK3 is highly expressed in the pre-BötC (**Paarmann et al., 2000**) and is calcium permeable (**Perrais et al., 2009**) making it a possible candidate for synaptically mediated calcium entry. Furthermore, GluK3 is insensitive to tonic glutamate release and only activated by large glutamate transients (**Perrais et al., 2009**). Consequently, GluK3 may only be activated when receiving synaptic input from a bursting presynaptic neuron which would presumably generate large glutamate transients. The role of GluK3 in the pre-BötC has not been investigated.

Metabotropic glutamate receptors (mGluR) indirectly activate ion channels through G-protein mediated signaling cascades. Group 1 mGluRs which include mGluR1 and mGluR5 are typically located on post-synaptic terminals (**Shigemoto et al., 1997**) and activation of group 1 mGluRs is commonly associated with calcium influx through calcium permeable channels (**Berg et al., 2007**; **Endoh, 2004**; **Mironov, 2008**) and calcium release from intracellular calcium stores (**Pace et al., 2007**).

In the pre-BötC, mGluR1/5 are thought to contribute to calcium influx by triggering the release of calcium from intracellular stores (**Pace et al., 2007**) and/or the activation of the transient receptor potential C3 (TRPC3) channel (**Ben-Mabrouk and Tryba, 2010**). Blockade of mGluR1/5 reduces the inspiratory drive potential in pre-BötC neurons (**Pace et al., 2007**) without significant perturbation of inspiratory frequency (**Pace et al., 2007**; **Lieske and Ramirez, 2006a**), which is consistent with the effects of I_{CAN}/TRPM4 blockade (**Koizumi et al., 2018**). TRPC3 is a calcium permeable channel (**Thebault et al., 2005**) that is associated with calcium signaling (**Hartmann et al., 2011**), store-operated calcium entry (**Kwan et al., 2004**), and synaptic transmission (**Hartmann et al., 2011**). TRPC3 is activated by diacylglycerol (DAG) (**Clapham, 2003**), which is formed after synaptic activation of mGluR1/5. TRPC3, which is highly expressed in pre-BötC glutamatergic inspiratory neurons, is often co-expressed with TRPM4 (**Koizumi et al., 2018**) and was hypothesized to underlie I_{CAN} activation in the pre-BötC (**Ben-Mabrouk and Tryba, 2010**) and other brain regions (**Amaral and Pozzo-Miller, 2007**; **Zitt et al., 1997**). Furthermore, TRPC3 and I_{CAN} have been shown to underlie slow excitatory post-synaptic current (sEPSC) (**Hartmann et al., 2008**; **Hartmann et al., 2011**). This is consistent with our model since I_{CAN} activation is dependent on synaptically triggered calcium entry, and the calcium dynamics are slower than the fast AMPA based current I_{Syn}. Therefore, in our model, I_{CAN} decays relatively slowly and, hence, can be treated as a sEPSC.

The effect of TRPC3 blockade by 3-pyrazole on pre-BötC network activity amplitude is remarkably similar to that with blockade of TRPM4 (**Koizumi et al., 2018**). This suggests that the I_{CAN}/TRPM4 activation may be dependent on/coupled to TRPC3. A possible explanation is that TRPC3, which is calcium permeable, mediates synaptically triggered calcium entry. It is also likely that TRPC3 plays a role in maintaining background calcium concentration levels. We tested this hypothesis by simulating the blockade of synaptically-triggered calcium influx while simultaneously lowering the background calcium concentration (**Figure 11**). These simulations generated large reductions in activity amplitude with no effect on frequency which are consistent with data from experiments where TRPC3 is blocked using 3-pyrazole (**Koizumi et al., 2018**). This indirectly suggests that TRPC3 may be critical for synaptically-triggered calcium entry and subsequent I_{CAN} activation.

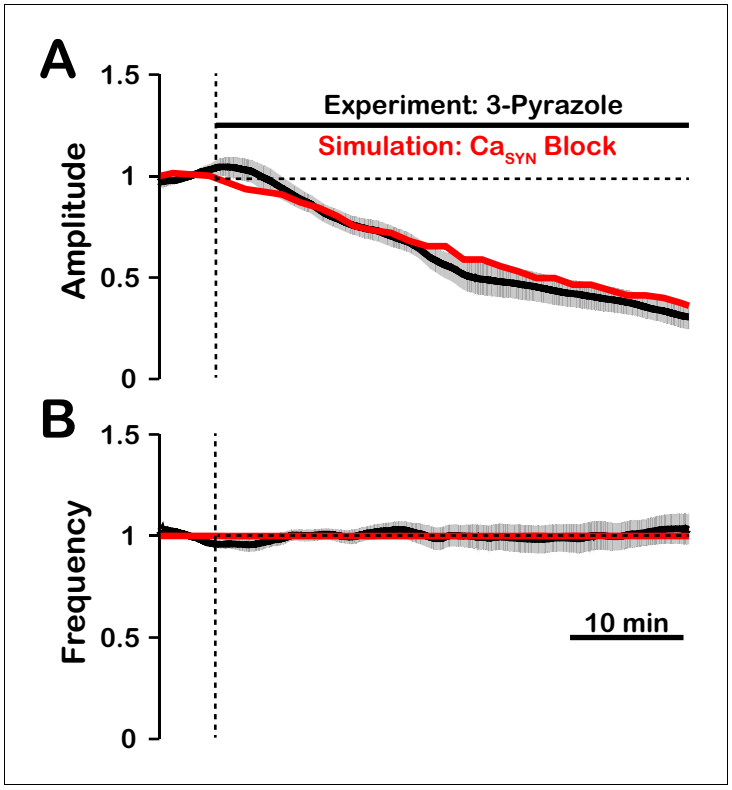

Figure 11. Comparison of experimental (black) and simulated (red) TRPC3 blockade (by Ca_{Syn} block) on network activity amplitude (A) and frequency (B). Simulated and experimental blockade begins at the vertical dashed line. The black line represents the mean and the gray band represents the S.E.M. of experimental integrated XII output recorded from neonatal rat brainstem slices in vitro, reproduced from ***Koizumi et al., 2018***. Blockade was simulated by exponential decay of P_{Ca} with the following parameters: 3-pyrazole: $\gamma_{Block} = 1.0$, $\tau_{Block} = 522.5\,s$. The network parameters are: $\bar{g}_{Ca} = 0.00175$ (nS), $P_{Ca} = 0.0275$, $P_{Syn} = 0.05$ and $W_{max} = 0.096$ (nS).
DOI: https://doi.org/10.7554/eLife.41555.012

I_{NaP} -dependent rhythmogenic kernel

I_{NaP} is a conductance present ubiquitously in pre-BötC inspiratory neurons, and is established to underlie intrinsic oscillatory neuronal bursting in the absence of excitatory synaptic interactions in neurons with sufficiently high I_{NaP} conductance densities (***Del Negro et al., 2002***; ***Koizumi and Smith, 2008***; ***Koizumi and Smith, 2008***; ***Yamanishi et al., 2018***). Accordingly, we randomly incorporated this conductance in our model excitatory neurons from a uniform statistical distribution to produce heterogeneity in I_{NaP} conductance density across the population. Our simulations indicate that the circuit neurons mostly with relatively high I_{NaP} conductance values underlie rhythm generation and remain active after compete blockade of I_{CAN} in our model network, thus forming a I_{NaP}-dependent rhythmogenic kernel, including some neurons with intrinsic oscillatory bursting behavior when synaptically uncoupled.

As noted above, the rhythmogenic properties of individual neurons depend on whether their I_{NaP} conductance is high enough and, therefore, the number of intrinsic bursters in the model is defined by the width of this conductance distribution over the population. However, the critical value of I_{NaP} conductance and intrinsic bursting properties in general were also shown theoretically and experimentally to critically depend on the conductances of other ionic channels (e.g. leak and delayed rectifier potassium conductances) and extracellular ion concentrations such as potassium concentration (***Bacak et al., 2016b***; ***Koizumi and Smith, 2008***; ***Rybak et al., 2003***). Therefore, we believe that in reality the specific composition of the rhythmogenic kernel and its oscillatory capabilities strongly depend on the existing combination of neuronal conductances and on the in vitro experimental conditions.

Recently, it has become apparent that there is functional heterogeneity within pre-BötC excitatory circuits, including distinct subpopulations of neurons involved in generating periodic sighs (**Toporikova et al., 2015**; **Li et al., 2016**), arousal (**Yackle et al., 2017**), and the subpopulations generating regular inspiratory activity. Activity of the normal inspiratory and sigh-generating subpopulations in the pre-BötC isolated in vitro is proposed to be dependent on activation of I_{NaP} (**Toporikova et al., 2015**). Our experimental and modeling results suggest that within the normal inspiratory population, there are subpopulations distinguished by their role in rhythm versus amplitude generation due to biophysical properties: there is a I_{CAN}/TRPM4-dependent recruitable population of excitatory neurons for burst amplitude generation and the I_{NaP}-dependent rhythmogenic kernel population. The spatial arrangements of these two synaptically interconnected excitatory populations within the pre-BötC are currently unknown, and it remains an important experimental problem to identify the cells constituting the rhythmogenic kernel and their biophysical properties. This should now be possible, since our analysis and experimental results suggest that the rhythmically active neurons of the kernel population can be revealed and studied after pharmacologically inhibiting the I_{CAN}/TRPM4-dependent inspiratory burst-generating population.

A 'burstlet theory' for emergent network rhythms has recently been proposed to account for inspiratory rhythm and pattern generation in the isolated pre-BötC in vitro (**Kam et al., 2013**; **Del Negro et al., 2018**). This theory postulates that a subpopulation of excitatory neurons generating small amplitude oscillations (burstlets) functions as the inspiratory rhythm generator that drives neurons that generate the larger amplitude, synchronized inspiratory population bursts. This concept emphasizes that subthreshold neuronal membrane oscillations need to be considered and that there is a neuronal subpopulation that functions to independently form the main inspiratory bursts. This is similar to our concept of distinct excitatory subpopulations generating the rhythm versus the amplitude of inspiratory oscillations. Biophysical mechanisms generating rhythmic burstlets and the large amplitude inspiratory population bursts in the burstlet theory are unknown, and the general problem of understanding the dynamic interplay of circuit interactions and cellular biophysical processes in the generation of population-level bursting activity has been highlighted (**Richter and Smith, 2014**; **Ramirez and Baertsch, 2018b**). We have identified a major Ca^{2+}-dependent conductance mechanism for inspiratory burst amplitude (pattern) generation and show theoretically how this mechanism may be coupled to excitatory synaptic interactions and is independent of the rhythm-generating mechanism. We also note that a basic property of I_{NaP} is its ability to generate subthreshold oscillations and promote burst synchronization (**Butera et al., 1999b**; **Bacak et al., 2016a**). However, in contrast to our proposal for the mechanisms operating in the kernel rhythm-generating subpopulation, I_{NaP} with its favorable voltage-dependent and kinetic autorhythmic properties– is not proposed to be a basic biophysical mechanism for rhythm generation in the burstlet theory (**Del Negro et al., 2018**).

We emphasize that the above discussions regarding the role of I_{NaP} pertain to the excitatory circuits in the isolated pre-BötC including in more mature rodent experimental preparations in situ where inspiratory rhythm generation has also been shown to be dependent on I_{NaP} (**Smith et al., 2007**). The analysis is more complex when the pre-BötC is embedded within interacting respiratory circuits in the intact nervous system generating the full complement of inspiratory and expiratory phase activity (**Lindsey et al., 2012**; **Ramirez and Baertsch, 2018a**; **Richter and Smith, 2014**), where rhythmogenesis is tightly controlled by inhibitory circuit interactions, including via local inhibitory circuits in the pre-BötC (**Harris et al., 2017**; **Ausborn et al., 2018**; **Baertsch et al., 2018**; **Ramirez and Baertsch, 2018a**), and the contribution of I_{NaP} kinetic properties alone in setting the timing of inspiratory oscillations is diminished (**Smith et al., 2007**; **Richter and Smith, 2014**; **Rubin et al., 2009b**). Extending our analysis to consider inhibitory circuit interactions with the excitatory subpopulations generating oscillation frequency and amplitude that we propose will provide additional insight into biophysical mechanisms controlling these two processes.

Conclusions

Based on our computational model, distinct biophysical mechanisms are involved in generating the rhythm and amplitude of inspiratory oscillations in the isolated pre-BötC excitatory circuits. According to this model, inspiratory rhythm generation arises from a group of I_{NaP}-dependent excitatory neurons, including cells with intrinsic oscillatory bursting properties, that form a rhythmogenic kernel. Rhythmic synaptic drive from these neurons triggers post-synaptic calcium transients,

I_{CAN} activation, and subsequent membrane depolarization which drives rhythmic bursting in the rest of the population of inspiratory neurons. We showed that activation of I_{CAN} by synaptically-driven calcium influx functions as a mechanism that amplifies the excitatory synaptic input to generate the inspiratory drive potential and population activity amplitude in these non-rhythmogenic neurons. Consequently, reduction of I_{CAN} causes a robust decrease in overall network activity amplitude via de-recruitment of these burst amplitude-generating neurons without substantial perturbations of the inspiratory rhythm. Thus, I_{CAN} plays a critical role in generating the amplitude of rhythmic population activity, which is consistent with the results from experimental inhibition of I_{CAN}/TRPM4 channels (**Peña et al., 2004**; **Koizumi et al., 2018**). Our model provides a theoretical explanation for these experimental results and new insights into the biophysical operation of pre-BötC excitatory circuits. The theoretical framework that we have developed here should provide the bases for further exploration of biophysical mechanisms operating in the mammalian respiratory oscillator.

Materials and methods

Model description

The model describes a network of $N = 100$ synaptically coupled excitatory neurons. Simulated neurons are comprised of a single compartment described using a Hodgkin Huxley formalism. For each neuron, the membrane potential V_m is given by the following current balance equation:

$$C_m \frac{dV_m}{dt} + I_{Na} + I_K + I_{Leak} + I_{NaP} + I_{CAN} + I_{Ca} + I_{Syn} = 0$$

where C_m is the membrane capacitance, I_{Na}, I_K, I_{Leak}, I_{NaP}, I_{CAN}, I_{Ca} and I_{Syn} are ionic currents through sodium, potassium, leak, persistent sodium, calcium activated non-selective cation, voltage-gated calcium, and synaptic channels, respectively. Description of these currents, synaptic interactions, and parameter values are taken from **Jasinski et al. (2013)**. The channel currents are defined as follows:

$$I_{Na} = \bar{g}_{Na} \cdot m_{Na}^3 \cdot h_{Na} \cdot (V_m - E_{Na})$$

$$I_K = \bar{g}_K \cdot m_K^4 \cdot (V_m - E_K)$$

$$I_{Leak} = \bar{g}_{Leak} \cdot (V_m - E_{Leak})$$

$$I_{NaP} = \bar{g}_{NaP} \cdot m_{NaP} \cdot h_{NaP} \cdot (V_m - E_{Na})$$

$$I_{CAN} = \bar{g}_{CAN} \cdot m_{CAN} \cdot (V_m - E_{CAN})$$

$$I_{Ca} = \bar{g}_{Ca} \cdot m_{Ca} \cdot h_{Ca} \cdot (V_m - E_{Ca})$$

$$I_{Syn} = g_{Syn} \cdot (V_m - E_{Syn})$$

where $\bar{g}_i$ is the maximum conductance, E_i is the reversal potential, m_i and h_i are voltage dependent gating variables for channel activation and inactivation, respectively, and $i \in \{Na, K, Leak, NaP, CAN, Ca, Syn\}$. The parameters $\bar{g}_i$ and E_i are given in **Table 1**.

For I_{Na}, I_K, I_{NaP}, and I_{Ca}, the dynamics of voltage-dependent gating variables m_i, and h_i are defined by the following differential equation:

$$\tau_\eta(V) \cdot \frac{d\eta}{dt} = \eta_\infty(V) - \eta;\ \eta \in \{m_i, h_i\}$$

where steady state activation/inactivation η_∞ and time constant τ_η are given by:

$$\eta_\infty(V) = \left(1 + e^{-\left(V - V_{\eta_{1/2}}\right)/k_\eta}\right)^{-1}$$

$$\tau_\eta(V) = \tau_{\eta_{max}} / \cosh\left(\left(V - V_{\tau\eta_{1/2}}\right)/k_{\tau_\eta}\right).$$

For the voltage-gated potassium channel, steady state activation $m_{K\infty}(V)$ and time constant $\tau_{mK}(V)$ are given by:

$$m_{K\infty}(V) = \frac{\alpha_\infty(V)}{\alpha_\infty(V) + \beta_\infty(V)}$$

$$\tau_{mK}(V) = 1/(\alpha_\infty(V) + \beta_\infty(V))$$

where

$$\alpha_\infty(V) = A_\alpha \cdot (V + B_\alpha)/(1 - exp(-(V + B_\alpha)/\kappa_\alpha))$$

$$\beta_\infty(V) = A_\beta \cdot exp\left(-\left(V + B_\beta\right)/\kappa_\beta\right).$$

The parameters $V_{\eta_{1/2}}$, $V_{\tau\eta_{1/2}}$, κ_η, $\kappa_{\tau\eta}$ $\tau_{\eta max}$, A_α, A_β, B_α, B_β, κ_α, and κ_β are given in **Table 1**. I_{CAN} activation is dependent on the intracellular calcium concentration $[Ca]_{in}$ and is given by:

$$m_{CAN} = 1/\left(1 + \left(Ca_{1/2}/[Ca]_{in}\right)^n\right).$$

The parameters $Ca_{1/2}$ and n, given in **Table 1**, represent the half-activation calcium concentration and the Hill Coefficient, respectively.

Calcium enters the neurons through voltage-gated calcium channels (Ca_V) and/or synaptic channels (Ca_{Syn}), where a percentage (P_{Ca}) of the synaptic current (I_{Syn}) is assumed to consist of Ca^{2+} ions. A calcium pump removes excess calcium with a time constant τ_{Ca} and sets the minimum calcium concentration Ca_{min}. The dynamics of $[Ca]_{in}$ is given by the following differential equation:

$$\frac{d[Ca]_{in}}{dt} = -\alpha_{Ca}\left(I_{Ca} + P_{Ca} \cdot I_{syn}\right) - \left([Ca]_{in} - Ca_{min}\right)/\tau_{Ca}.$$

The parameters α_{Ca} is a conversion factor relating current and rate of change in $[Ca]_{in}$, see **Table 1** for parameter values.

The synaptic conductance of the i^{th} neuron (g^i_{Syn}) in the population is described by the following equation:

$$g^i_{Syn} = g_{Tonic} + \sum_{j,n} w_{ji} \cdot C_{ji} \cdot H\left(t - t_{j,n}\right) \cdot e^{-\left(t - t_{j,n}\right)/\tau_{syn}}$$

where w_{ji} is the weight of the synaptic connection from cell j to cell i, C is a connectivity matrix ($C_{ji} = 1$ if neuron j makes a synapse on neuron i, and $C_{ji} = 0$ otherwise), $H(.)$ is the Heaviside step function, t is time, τ_{Syn} is the exponential decay constant and $t_{j,n}$ is the time at which an action potential n is generated in neuron j and reaches neuron i.

To account for heterogeneity of neuron properties within the network, the persistent sodium current conductance, $\bar{g}_{NaP}$, for each neuron was assigned randomly based on a uniform distribution over the range $[0.0, 5.0]$ nS which is consistent with experimental measurements (**Rybak et al., 2003**; **Koizumi and Smith, 2008**; **Koizumi and Smith, 2008**). We also uniformly distributed $\bar{g}_{CAN}$ over the range $[0.5, 1.5]$ nS , however, simulation results did not depend on whether we used such a distribution, or assigned $\bar{g}_{CAN}$ for all neurons to the same value of 1.0 nS, which is the mean of this distribution. In simulations where $\bar{g}_{CAN}$ was varied, we multiplied $\bar{g}_{CAN}$ for each neuron by the same factor. This factor was used as a control parameter for all such simulations, and shown as a percentage of the baseline $\bar{g}_{CAN}$ or as the mean $\bar{g}_{CAN}$ values for the population in figures. The weight of each synaptic connection was uniformly distributed over the range $w_{ji} \in [0, W_{max}]$ where W_{max} ranged from 0.0 to 1.0 nS depending on the network connectivity and specific simulation. The elements of the network connectivity matrix, C_{ji}, are randomly assigned values of 0 or 1 such that the probability of any connection between neuron j and neuron i being 1 is equal to the network connection probability P_{Syn}.

Table 1. Model parameter values.
The channel kinetics, intracellular Ca^{2+} dynamics and the corresponding parameter values, were derived from previous models (see ***Jasinski et al., 2013***) and the references therein).

Channel	Parameters
I_{Na}	$\bar{g}_{Na} = 150.0\ nS,\ E_{Na} = 55.0\ mV,$ $V_{m_{1/2}} = -43.8\,mV,\ k_m = 6.0\ mV,$ $V_{\tau m_{1/2}} = -43.8\ mV,\ k_{\tau_m} = 14.0\ mV,\ \tau_{m_{max}} = 0.25\ ms,$ $V_{h_{1/2}} = -67.5\,mV,\ k_h = -10.8\ mV,$ $V_{\tau h_{1/2}} = -67.5\ mV,\ k_{\tau_h} = 12.8\ mV,\ \tau_{h_{max}} = 8.46\ ms$
I_K	$\bar{g}_K = 160.0\ nS,\ E_K = -94.0\ mV,$ $A_\alpha = 0.01,\ B_\alpha = 44.0\ mV,\ \kappa_\alpha = 5.0\ mV$ $A_\beta = 0.17,\ B_\beta = 49.0\ mV,\ \kappa_\beta = 40.0\ mV$
I_{Leak}	$\bar{g}_{Leak} = 2.5\ nS,\ E_{Leak} = -68.0\ mV$
I_{NaP}	$\bar{g}_{NaP} \in [0.0, 5.0]\ nS,$ $V_{m_{1/2}} = -47.1\,mV,\ k_m = 3.1\ mV,$ $V_{\tau m_{1/2}} = -47.1\ mV,\ k_{\tau_m} = 6.2\ mV,\ \tau_{m_{max}} = 1.0\ ms,$ $V_{h_{1/2}} = -60.0\,mV,\ k_h = -9.0\ mV,$ $V_{\tau h_{1/2}} = -60.0\ mV,\ k_{\tau_h} = 9.0\ mV,\ \tau_{h_{max}} = 5000\ ms$
I_{CAN}	$\bar{g}_{CAN} \in [0.5, 1.5]\ nS,\ E_{CAN} = 0.0\ mV,$ $Ca_{1/2} = 0.00074\ mM,\ n = 0.97$
I_{Ca}	$\bar{g}_{Ca} = 0.01\ nS,\ E_{Ca} = R \cdot T/F \cdot ln\left([Ca]_{out}/[Ca]_{in}\right),$ $R = 8.314\ J/(mol \cdot K),\ T = 308.0\ K,$ $F = 96.485\ kC/mol,\ [Ca]_{out} = 4.0\ mM$ $V_{m_{1/2}} = -27.5\,mV,\ k_m = 5.7\ mV,\ \tau_m = 0.5\ ms,$ $V_{h_{1/2}} = -52.4\,mV,\ k_h = -5.2\ mV,\ \tau_h = 18.0\ ms$
Ca_{in}	$\alpha_{Ca} = 2.5 \cdot 10^{-5} mM/fC,\ P_{Ca} = 0.01,\ Ca_{min} = 1.0 \cdot 10^{-10} mM,\ \tau_{Ca} = 50.0\,ms$
I_{Syn}	$g_{Tonic} = 0.31\ nS,\ E_{Syn} = -10.0\ mV,\ \tau_{Syn} = 5.0\ ms$

DOI: https://doi.org/10.7554/eLife.41555.013

We varied the connection probability over the range $P_{Syn} \in [0.05, 1.0]$, however, a value of $P_{Syn} = 0.05$ was used in most simulations.

Data analysis and definitions

The time of an action potential was defined as when the membrane potential of a neuron crosses $-35mV$ in a positive direction. The network activity amplitude and frequency were determined by identifying peaks and calculating the inverse of the interpeak interval in histograms of network spiking. Network histograms of the population activity were calculated as the number of action potentials generated by all neurons per 50 *ms* bin per neuron with units of $spikes/s$. The number of recruited neurons is defined as the peak number of neurons that spiked at least once per bin during a network burst. The average spike frequency of recruited neurons is defined as the number of action potentials per bin per recruited neuron with units of $spikes/s$. The average network resting membrane potential was defined as the average minimum value of V_m in a 500 ms window following a network burst. The average inactivation of the persistent sodium current at the start of each burst was defined by the maximum of the average value of h_{NaP} in a 500-ms window before the peak of each network burst. The average inactivation of the persistent sodium current at the end of each burst was defined by the maximum of the average value of h_{NaP} in a 500-ms window after the peak of each network burst. Synaptic strength is defined as the number of neurons in the network multiplied by the connection probability multiplied by the average weight of synaptic connections ($N \cdot P_{Syn} \cdot \frac{1}{2} W_{max}$). Pacemaker neurons were defined as neurons that continue bursting intrinsically after complete synaptic blockade. Follower neurons were defined as neurons that become silent after complete synaptic blockade. The inspiratory drive potential is defined as the envelope of depolarization that occurs in neurons during the inspiratory phase of the network oscillations (***Morgado-Valle et al., 2008***).

Characterization of I_{CAN} in regulating network activity amplitude and frequency in Ca_V and Ca_{Syn} models

To characterize the role of I_{CAN} in regulation of network activity amplitude and frequency we slowly increased the conductance ($\bar{g}_{CAN}$) in our simulations from zero until the network transitioned from a rhythmic bursting to a tonic (non-bursting) firing regime. To ensure that the effect(s) are robust, these simulations were repeated over a wide range of synaptic weights, synaptic connection probabilities, and strengths of the intracellular calcium transients from Ca_V or Ca_{Syn} sources. Changes in network activity amplitude were further examined by plotting the number of recruited neurons and the average action potential frequency of recruited neurons versus $\bar{g}_{CAN}$.

Simulated pharmacological manipulations

In simulations that are compared with experimental data, both Ca_V and Ca_{Syn} calcium sources are included. Pharmacological blockade of I_{CAN} was simulated by varying the conductance, $\bar{g}_{CAN}$ according to a decaying exponential function

$$\bar{g}_{CAN}(t) = g_{CAN}^{max} - \gamma_{block} \cdot \left(1 - e^{-t/\tau_{block}}\right).$$

The percent block γ_{block}, decay constant τ_{block} and the maximum I_{CAN} conductance g_{CAN}^{max} were adjusted to match the experimental changes in network amplitude. The synaptic weight of the network was chosen such that at $\bar{g}_{CAN} = 0$ the network activity amplitude was close to 20% of maximum. To reduce the computational time, the duration of I_{CAN} block simulations was one tenth of the total of experimental durations. For comparison, the plots of normalized change in amplitude and frequency of the simulations were stretched over the same time-period as experimental data. Increasing the simulation time had no effect on our results (data not shown).

Comparison with calcium imaging data

To allow comparisons with network and cellular calcium imaging data, we analyzed rhythmic calcium transients from our simulations. Single cell calcium signals are represented by $[Ca]_i$. The network calcium signal was calculated as the average intracellular calcium concentration in the network $(\sum_{1}^{N}[Ca]_i/N)$.

Integration methods

All simulations were performed locally on an 8-core Linux-based operating system or on the high-performance computing cluster Biowulf at the National Institutes of Health. Simulation software was custom written in C++. Numerical integration was performed using the exponential Euler method with a fixed step-size (Δt) of $0.025\,ms$. In all simulations, the first 50 s of simulation time was discarded to allow for the decay of any initial condition-dependent transients.

Acknowledgements

This work was supported in part by the Jayne Koskinas and Ted Giovanis Foundation for Health and Policy, the Intramural Research Program of the National Institutes of Health (NIH), National Institute of Neurological Disorders and Stroke (NINDS), and NIH Grants R01 AT008632 and U01 EB021960.

Additional information

Funding

Funder	Grant reference number	Author
The Jayne Koskinas Ted Giovanis Foundation for Health and Policy		Ryan S Phillips
National Institute of Neurological Disorders and Stroke	Intramural Research Program of the National Institutes of Health	Ryan S Phillips Tibin T John Hidehiko Koizumi Jeffrey C Smith

National Institutes of Health	R01 AT008632	Yaroslav I Molkov
National Institutes of Health	U01 EB021960	Yaroslav I Molkov

The funders had no role in study design, data collection and interpretation, or the decision to submit the work for publication.

Author contributions

Ryan S Phillips, Yaroslav I Molkov, Jeffrey C Smith, Conceptualization, Data curation, Formal analysis, Writing—original draft, Writing—review and editing; Tibin T John, Hidehiko Koizumi, Data curation, Formal analysis

Author ORCIDs

Ryan S Phillips http://orcid.org/0000-0002-8570-2348
Tibin T John http://orcid.org/0000-0002-6825-7166
Yaroslav I Molkov http://orcid.org/0000-0002-0862-1974
Jeffrey C Smith http://orcid.org/0000-0002-7676-4643

Decision letter and Author response

Decision letter https://doi.org/10.7554/eLife.41555.017
Author response https://doi.org/10.7554/eLife.41555.018

Additional files

Supplementary files

- Source code 1. Phillips et al. model source code.

DOI: https://doi.org/10.7554/eLife.41555.014

- Transparent reporting form

DOI: https://doi.org/10.7554/eLife.41555.015

Data availability

All data in this study are generated by computational simulations. All model parameters and equations are included in the manuscript and source code is included with this submission.

References

Amaral MD, Pozzo-Miller L. 2007. TRPC3 channels are necessary for brain-derived neurotrophic factor to activate a nonselective cationic current and to induce dendritic spine formation. *Journal of Neuroscience* **27**:5179–5189. DOI: https://doi.org/10.1523/JNEUROSCI.5499-06.2007, PMID: 17494704

Ausborn J, Koizumi H, Barnett WH, John TT, Zhang R, Molkov YI, Smith JC, Rybak IA. 2018. Organization of the core respiratory network: insights from optogenetic and modeling studies. *PLOS Computational Biology* **14**: e1006148. DOI: https://doi.org/10.1371/journal.pcbi.1006148, PMID: 29698394

Bacak BJ, Kim T, Smith JC, Rubin JE, Rybak IA. 2016a. Mixed-mode oscillations and population bursting in the pre-Bötzinger complex. *eLife* **5**:e13403. DOI: https://doi.org/10.7554/eLife.13403, PMID: 26974345

Bacak BJ, Segaran J, Molkov YI. 2016b. Modeling the effects of extracellular potassium on bursting properties in pre-Bötzinger complex neurons. *Journal of Computational Neuroscience* **40**:231–245. DOI: https://doi.org/10.1007/s10827-016-0594-8, PMID: 26899961

Baertsch NA, Baertsch HC, Ramirez JM. 2018. The interdependence of excitation and inhibition for the control of dynamic breathing rhythms. *Nature Communications* **9**:843. DOI: https://doi.org/10.1038/s41467-018-03223-x, PMID: 29483589

Beltran-Parrazal L, Fernandez-Ruiz J, Toledo R, Manzo J, Morgado-Valle C. 2012. Inhibition of endoplasmic reticulum Ca^{2+} ATPase in preBötzinger complex of neonatal rat does not affect respiratory rhythm generation. *Neuroscience* **224**:116–124. DOI: https://doi.org/10.1016/j.neuroscience.2012.08.016, PMID: 22906476

Ben-Mabrouk F, Tryba AK. 2010. Substance P modulation of TRPC3/7 channels improves respiratory rhythm regularity and ICAN-dependent pacemaker activity. *European Journal of Neuroscience* **31**:1219–1232. DOI: https://doi.org/10.1111/j.1460-9568.2010.07156.x, PMID: 20345918

Berg AP, Sen N, Bayliss DA. 2007. TrpC3/C7 and Slo2.1 are molecular targets for metabotropic glutamate receptor signaling in rat striatal cholinergic interneurons. *Journal of Neuroscience* **27**:8845–8856. DOI: https://doi.org/10.1523/JNEUROSCI.0551-07.2007, PMID: 17699666

Butera RJ, Rinzel J, Smith JC. 1999a. Models of respiratory rhythm generation in the pre-Bötzinger complex. I. bursting pacemaker neurons. *Journal of Neurophysiology* **82**:382–397. DOI: https://doi.org/10.1152/jn.1999.82.1.382, PMID: 10400966

Butera RJ, Rinzel J, Smith JC. 1999b. Models of respiratory rhythm generation in the pre-Bötzinger complex. II. populations of coupled pacemaker neurons. *Journal of Neurophysiology* **82**:398–415. DOI: https://doi.org/10.1152/jn.1999.82.1.398, PMID: 10400967

Buzsaki G. 2006. *Rhythms of the Brain*. Oxford University Press. DOI: https://doi.org/10.1093/acprof:oso/9780195301069.001.0001

Carroll MS, Viemari JC, Ramirez JM. 2013. Patterns of inspiratory phase-dependent activity in the in vitro respiratory network. *Journal of Neurophysiology* **109**:285–295. DOI: https://doi.org/10.1152/jn.00619.2012, PMID: 23076109

Carroll MS, Ramirez JM. 2013. Cycle-by-cycle assembly of respiratory network activity is dynamic and stochastic. *Journal of Neurophysiology* **109**:296–305. DOI: https://doi.org/10.1152/jn.00830.2011, PMID: 22993257

Chevalier M, Toporikova N, Simmers J, Thoby-Brisson M. 2016. Development of pacemaker properties and rhythmogenic mechanisms in the mouse embryonic respiratory network. *eLife* **5**:e16125. DOI: https://doi.org/10.7554/eLife.16125, PMID: 27434668

Clapham DE. 2003. TRP channels as cellular sensors. *Nature* **426**:517–524. DOI: https://doi.org/10.1038/nature02196, PMID: 14654832

Del Negro CA, Koshiya N, Butera RJ, Smith JC. 2002. Persistent sodium current, membrane properties and bursting behavior of pre-bötzinger complex inspiratory neurons in vitro. *Journal of Neurophysiology* **88**:2242–2250. DOI: https://doi.org/10.1152/jn.00081.2002, PMID: 12424266

Del Negro CA, Morgado-Valle C, Hayes JA, Mackay DD, Pace RW, Crowder EA, Feldman JL. 2005. Sodium and calcium current-mediated pacemaker neurons and respiratory rhythm generation. *Journal of Neuroscience* **25**:446–453. DOI: https://doi.org/10.1523/JNEUROSCI.2237-04.2005, PMID: 15647488

Del Negro CA, Hayes JA, Pace RW, Brush BR, Teruyama R, Feldman JL. 2010. Synaptically activated burst-generating conductances may underlie a group-pacemaker mechanism for respiratory rhythm generation in mammals. *Progress in Brain Research* **187**:111–136. DOI: https://doi.org/10.1016/B978-0-444-53613-6.00008-3, PMID: 21111204

Del Negro CA, Funk GD, Feldman JL. 2018. Breathing matters. *Nature Reviews Neuroscience* **19**:351–367. DOI: https://doi.org/10.1038/s41583-018-0003-6, PMID: 29740175

Endoh T. 2004. Characterization of modulatory effects of postsynaptic metabotropic glutamate receptors on calcium currents in rat nucleus tractus solitarius. *Brain Research* **1024**:212–224. DOI: https://doi.org/10.1016/j.brainres.2004.07.074, PMID: 15451384

Feldman JL, Del Negro CA. 2006. Looking for inspiration: new perspectives on respiratory rhythm. *Nature Reviews Neuroscience* **7**:232–241. DOI: https://doi.org/10.1038/nrn1871, PMID: 16495944

Grillner S. 2006. Biological pattern generation: the cellular and computational logic of networks in motion. *Neuron* **52**:751–766. DOI: https://doi.org/10.1016/j.neuron.2006.11.008, PMID: 17145498

Guinamard R, Demion M, Launay P. 2010. Physiological roles of the TRPM4 channel extracted from background currents. *Physiology* **25**:155–164. DOI: https://doi.org/10.1152/physiol.00004.2010, PMID: 20551229

Harris KD, Dashevskiy T, Mendoza J, Garcia AJ, Ramirez JM, Shea-Brown E. 2017. Different roles for inhibition in the rhythm-generating respiratory network. *Journal of Neurophysiology* **118**:2070–2088. DOI: https://doi.org/10.1152/jn.00174.2017, PMID: 28615332

Hartmann J, Dragicevic E, Adelsberger H, Henning HA, Sumser M, Abramowitz J, Blum R, Dietrich A, Freichel M, Flockerzi V, Birnbaumer L, Konnerth A. 2008. TRPC3 channels are required for synaptic transmission and motor coordination. *Neuron* **59**:392–398. DOI: https://doi.org/10.1016/j.neuron.2008.06.009, PMID: 18701065

Hartmann J, Henning HA, Konnerth A. 2011. mGluR1/TRPC3-mediated synaptic transmission and calcium signaling in mammalian central neurons. *Cold Spring Harbor Perspectives in Biology* **3**:a006726. DOI: https://doi.org/10.1101/cshperspect.a006726, PMID: 21441586

Jasinski PE, Molkov YI, Shevtsova NA, Smith JC, Rybak IA. 2013. Sodium and calcium mechanisms of rhythmic bursting in excitatory neural networks of the pre-Bötzinger complex: a computational modelling study. *European Journal of Neuroscience* **37**:212–230. DOI: https://doi.org/10.1111/ejn.12042

Johnson SM, Smith JC, Funk GD, Feldman JL. 1994. Pacemaker behavior of respiratory neurons in medullary slices from neonatal rat. *Journal of Neurophysiology* **72**:2598–2608. DOI: https://doi.org/10.1152/jn.1994.72.6.2598, PMID: 7897477

Kam K, Worrell JW, Ventalon C, Emiliani V, Feldman JL. 2013. Emergence of population bursts from simultaneous activation of small subsets of preBötzinger complex inspiratory neurons. *Journal of Neuroscience* **33**:3332–3338. DOI: https://doi.org/10.1523/JNEUROSCI.4574-12.2013, PMID: 23426661

Kiehn O. 2006. Locomotor circuits in the mammalian spinal cord. *Annual Review of Neuroscience* **29**:279–306. DOI: https://doi.org/10.1146/annurev.neuro.29.051605.112910, PMID: 16776587

Koch H, Zanella S, Elsen GE, Smith L, Doi A, Garcia AJ, Wei AD, Xun R, Kirsch S, Gomez CM, Hevner RF, Ramirez JM. 2013. Stable respiratory activity requires both P/Q-type and N-type voltage-gated calcium channels. *Journal of Neuroscience* **33**:3633–3645. DOI: https://doi.org/10.1523/JNEUROSCI.6390-11.2013, PMID: 23426690

Koizumi H, Wilson CG, Wong S, Yamanishi T, Koshiya N, Smith JC. 2008. Functional imaging, spatial reconstruction, and biophysical analysis of a respiratory motor circuit isolated in vitro. *Journal of Neuroscience* **28**:2353–2365. DOI: https://doi.org/10.1523/JNEUROSCI.3553-07.2008, PMID: 18322082

Koizumi H, John TT, Chia JX, Tariq MF, Phillips RS, Mosher B, Chen Y, Thompson R, Zhang R, Koshiya N, Smith JC. 2018. Transient receptor potential channels TRPM4 and TRPC3 critically contribute to respiratory motor pattern formation but not rhythmogenesis in rodent brainstem circuits. *eNeuro* **5**:ENEURO.0332-17.2018. DOI: https://doi.org/10.1523/ENEURO.0332-17.2018, PMID: 29435486

Koizumi H, Smith JC. 2008. Persistent na+ and K+-dominated leak currents contribute to respiratory rhythm generation in the pre-Bötzinger complex in vitro. *Journal of Neuroscience* **28**:1773–1785. DOI: https://doi.org/10.1523/JNEUROSCI.3916-07.2008, PMID: 18272697

Kwan HY, Huang Y, Yao X. 2004. Regulation of canonical transient receptor potential isoform 3 (TRPC3) channel by protein kinase G. *PNAS* **101**:2625–2630. DOI: https://doi.org/10.1073/pnas.0304471101, PMID: 14983059

Li P, Janczewski WA, Yackle K, Kam K, Pagliardini S, Krasnow MA, Feldman JL. 2016. The peptidergic control circuit for sighing. *Nature* **530**:293–297. DOI: https://doi.org/10.1038/nature16964, PMID: 26855425

Lieske SP, Ramirez JM. 2006a. Pattern-specific synaptic mechanisms in a multifunctional network. I. Effects of alterations in synapse strength. *Journal of Neurophysiology* **95**:1323–1333. DOI: https://doi.org/10.1152/jn.00505.2004, PMID: 16492944

Lieske SP, Ramirez JM. 2006b. Pattern-specific synaptic mechanisms in a multifunctional network. II. Intrinsic modulation by metabotropic glutamate receptors. *Journal of Neurophysiology* **95**:1334–1344. DOI: https://doi.org/10.1152/jn.00506.2004, PMID: 16492945

Lindsey BG, Rybak IA, Smith JC. 2012. Computational models and emergent properties of respiratory neural networks. *Comprehensive Physiology* **2**:1619–1670. DOI: https://doi.org/10.1002/cphy.c110016, PMID: 23687564

Marder E, Calabrese RL. 1996. Principles of rhythmic motor pattern generation. *Physiological Reviews* **76**:687–717. DOI: https://doi.org/10.1152/physrev.1996.76.3.687, PMID: 8757786

Mironov SL. 2008. Metabotropic glutamate receptors activate dendritic calcium waves and TRPM channels which drive rhythmic respiratory patterns in mice. *The Journal of Physiology* **586**:2277–2291. DOI: https://doi.org/10.1113/jphysiol.2007.149021, PMID: 18308826

Morgado-Valle C, Beltran-Parrazal L, DiFranco M, Vergara JL, Feldman JL. 2008. Somatic Ca2+ transients do not contribute to inspiratory drive in preBötzinger Complex neurons. *The Journal of Physiology* **586**:4531–4540. DOI: https://doi.org/10.1113/jphysiol.2008.154765, PMID: 18635649

Morgado-Valle C, Feldman JL. 2007. NMDA receptors in preBotzinger complex neurons can drive respiratory rhythm independent of AMPA receptors. *The Journal of Physiology* **582**:359–368. DOI: https://doi.org/10.1113/jphysiol.2007.130617, PMID: 17446224

Paarmann I, Frermann D, Keller BU, Hollmann M. 2000. Expression of 15 glutamate receptor subunits and various splice variants in tissue slices and single neurons of brainstem nuclei and potential functional implications. *Journal of Neurochemistry* **74**:1335–1345. DOI: https://doi.org/10.1046/j.1471-4159.2000.0741335.x, PMID: 10737588

Pace RW, Mackay DD, Feldman JL, Del Negro CA. 2007. Inspiratory bursts in the preBötzinger complex depend on a calcium-activated non-specific cation current linked to glutamate receptors in neonatal mice. *The Journal of Physiology* **582**:113–125. DOI: https://doi.org/10.1113/jphysiol.2007.133660, PMID: 17446214

Peña F, Parkis MA, Tryba AK, Ramirez JM. 2004. Differential contribution of pacemaker properties to the generation of respiratory rhythms during normoxia and hypoxia. *Neuron* **43**:105–117. DOI: https://doi.org/10.1016/j.neuron.2004.06.023, PMID: 15233921

Perrais D, Pinheiro PS, Jane DE, Mulle C. 2009. Antagonism of recombinant and native GluK3-containing kainate receptors. *Neuropharmacology* **56**:131–140. DOI: https://doi.org/10.1016/j.neuropharm.2008.08.002, PMID: 18761361

Pierrefiche O, Shevtsova NA, St-John WM, Paton JF, Rybak IA. 2004. Ionic currents and endogenous rhythm generation in the pre-Bötzinger complex: modelling and in vitro studies. *Advances in Experimental Medicine and Biology* **551**:121–126. DOI: https://doi.org/10.1007/0-387-27023-X_19, PMID: 15602953

Ramirez JM, Tryba AK, Peña F. 2004. Pacemaker neurons and neuronal networks: an integrative view. *Current Opinion in Neurobiology* **14**:665–674. DOI: https://doi.org/10.1016/j.conb.2004.10.011, PMID: 15582367

Ramirez JM, Baertsch N. 2018a. Defining the rhythmogenic elements of mammalian breathing. *Physiology* **33**:302–316. DOI: https://doi.org/10.1152/physiol.00025.2018, PMID: 30109823

Ramirez JM, Baertsch NA. 2018b. The dynamic basis of respiratory rhythm generation: one breath at a time. *Annual Review of Neuroscience* **41**:475–499. DOI: https://doi.org/10.1146/annurev-neuro-080317-061756, PMID: 29709210

Rekling JC, Feldman JL. 1998. PreBötzinger complex and pacemaker neurons: hypothesized site and kernel for respiratory rhythm generation. *Annual Review of Physiology* **60**:385–405. DOI: https://doi.org/10.1146/annurev.physiol.60.1.385, PMID: 9558470

Richter DW, Smith JC. 2014. Respiratory rhythm generation in vivo. *Physiology* **29**:58–71. DOI: https://doi.org/10.1152/physiol.00035.2013, PMID: 24382872

Rubin JE, Hayes JA, Mendenhall JL, Del Negro CA. 2009a. Calcium-activated nonspecific cation current and synaptic depression promote network-dependent burst oscillations. *PNAS* **106**:2939–2944. DOI: https://doi.org/10.1073/pnas.0808776106, PMID: 19196976

Rubin JE, Shevtsova NA, Ermentrout GB, Smith JC, Rybak IA. 2009b. Multiple rhythmic states in a model of the respiratory central pattern generator. *Journal of Neurophysiology* **101**:2146–2165. DOI: https://doi.org/10.1152/jn.90958.2008, PMID: 19193773

Rybak IA, Ptak K, Shevtsova NA, McCrimmon DR. 2003. Sodium currents in neurons from the rostroventrolateral medulla of the rat. *Journal of Neurophysiology* **90**:1635–1642. DOI: https://doi.org/10.1152/jn.00150.2003, PMID: 12761275

Rybak IA, Molkov YI, Jasinski PE, Shevtsova NA, Smith JC. 2014. Rhythmic bursting in the pre-Bötzinger complex: mechanisms and models. *Progress in Brain Research* **209**:1–23. DOI: https://doi.org/10.1016/B978-0-444-63274-6.00001-1, PMID: 24746040

Shigemoto R, Kinoshita A, Wada E, Nomura S, Ohishi H, Takada M, Flor PJ, Neki A, Abe T, Nakanishi S, Mizuno N. 1997. Differential presynaptic localization of metabotropic glutamate receptor subtypes in the rat hippocampus. *The Journal of Neuroscience* **17**:7503–7522. DOI: https://doi.org/10.1523/JNEUROSCI.17-19-07503.1997, PMID: 9295396

Smith JC, Ellenberger HH, Ballanyi K, Richter DW, Feldman JL. 1991. Pre-Bötzinger complex: a brainstem region that may generate respiratory rhythm in mammals. *Science* **254**:726–729. DOI: https://doi.org/10.1126/science.1683005, PMID: 1683005

Smith JC, Abdala AP, Koizumi H, Rybak IA, Paton JF. 2007. Spatial and functional architecture of the mammalian brain stem respiratory network: a hierarchy of three oscillatory mechanisms. *Journal of Neurophysiology* **98**:3370–3387. DOI: https://doi.org/10.1152/jn.00985.2007, PMID: 17913982

Smith JC, Abdala AP, Borgmann A, Rybak IA, Paton JF. 2013. Brainstem respiratory networks: building blocks and microcircuits. *Trends in Neurosciences* **36**:152–162. DOI: https://doi.org/10.1016/j.tins.2012.11.004, PMID: 23254296

Song H, Hayes JA, Vann NC, Drew LaMar M, Del Negro CA. 2015. Mechanisms leading to rhythm cessation in the respiratory PreBötzinger complex due to piecewise cumulative neuronal deletions. *eNeuro* **2**. DOI: https://doi.org/10.1523/ENEURO.0031-15.2015, PMID: 26465010

Thebault S, Zholos A, Enfissi A, Slomianny C, Dewailly E, Roudbaraki M, Parys J, Prevarskaya N. 2005. Receptor-operated Ca2+ entry mediated by TRPC3/TRPC6 proteins in rat prostate smooth muscle (PS1) cell line. *Journal of Cellular Physiology* **204**:320–328. DOI: https://doi.org/10.1002/jcp.20301, PMID: 15672411

Thoby-Brisson M, Ramirez JM. 2001. Identification of two types of inspiratory pacemaker neurons in the isolated respiratory neural network of mice. *Journal of Neurophysiology* **86**:104–112. DOI: https://doi.org/10.1152/jn.2001.86.1.104, PMID: 11431492

Toporikova N, Chevalier M, Thoby-Brisson M. 2015. Sigh and eupnea rhythmogenesis involve distinct interconnected subpopulations: a combined computational and experimental study. *eNeuro* **2**. DOI: https://doi.org/10.1523/ENEURO.0074-14.2015, PMID: 26464980

Toporikova N, Butera RJ. 2011. Two types of independent bursting mechanisms in inspiratory neurons: an integrative model. *Journal of Computational Neuroscience* **30**:515–528. DOI: https://doi.org/10.1007/s10827-010-0274-z, PMID: 20838868

Ullrich ND, Voets T, Prenen J, Vennekens R, Talavera K, Droogmans G, Nilius B. 2005. Comparison of functional properties of the Ca2+-activated cation channels TRPM4 and TRPM5 from mice. *Cell Calcium* **37**:267–278. DOI: https://doi.org/10.1016/j.ceca.2004.11.001, PMID: 15670874

Yackle K, Schwarz LA, Kam K, Sorokin JM, Huguenard JR, Feldman JL, Luo L, Krasnow MA. 2017. Breathing control center neurons that promote arousal in mice. *Science* **355**:1411–1415. DOI: https://doi.org/10.1126/science.aai7984, PMID: 28360327

Yamanishi T, Koizumi H, Navarro M, Milescu LS, Smith JC. 2018. Persistent sodium current kinetics orchestrate oscillatory burst firing in the pre-Bötzinger complex. *The Journal of General Physiology* **150**:1523–1540. DOI: https://doi.org/10.1085/jgp.201812100

Zitt C, Obukhov AG, Strübing C, Zobel A, Kalkbrenner F, Lückhoff A, Schultz G. 1997. Expression of TRPC3 in chinese hamster ovary cells results in calcium-activated cation currents not related to store depletion. *The Journal of Cell Biology* **138**:1333–1341. DOI: https://doi.org/10.1083/jcb.138.6.1333, PMID: 9298988